# Fourth-order self-energy contribution to the Lamb shift

S. Mallampalli and J. Sapirstein
*Department of Physics, University of Notre Dame, Notre Dame, Indiana 46556*
(Received 2 October 1997)

Two-loop self-energy contributions to the fourth-order Lamb shift of ground-state hydrogenic ions are treated to all orders in $Z\alpha$ by using exact Dirac-Coulomb propagators. A rearrangement of the calculation into four ultraviolet finite parts, the $M$, $P$, $F$, and perturbed orbital (PO) terms, is made. Reference-state singularities present in the $M$ and $P$ terms are shown to cancel. The most computationally intensive part of the calculation, the $M$ term, is evaluated for hydrogenlike uranium and bismuth, the $F$ term is evaluated for a range of $Z$ values, but the $P$ term is left for a future calculation. For hydrogenlike uranium, previous calculations of the PO term give $-0.971$ eV: the contributions from the $M$ and $F$ terms calculated here sum to $-0.325$ eV. [S1050-2947(98)00303-5]

PACS number(s): 12.20.−m

## INTRODUCTION

In a recent paper [1] we calculated the contribution of the two-loop vacuum polarization diagram of Fig. 1 for the ground state of hydrogenic ions using a method that treats the electron propagator in the presence of a point nucleus of charge $Z$, the Dirac-Coulomb propagator, exactly. One notable feature of the calculation was the strong $Z$ dependence exhibited: While at low $Z$ the first terms of the power series expansion in $Z\alpha$ approximated the complete calculation, at high $Z$ the answer was quite different. For example, if one sets $Z=92$ in the power series [2]

$$E^{4VP}(Z\alpha)=[0.014\,392-0.023\,208(Z\alpha)](Z\alpha)^4 \text{ a.u.} \quad (1)$$

$-0.000\,242$ a.u. results, while the exact answer is 0.004 939 a.u., an order of magnitude larger and of opposite sign.

In this paper we wish to extend our previous calculation to include the two-loop self-energy diagrams of Fig. 2. Figures 2(a) and 2(b) will be referred to in the following as the *nested* and *overlapping* diagrams respectively, following the notation of Ref. [3]. The reducible diagram shown in Fig. 2(c) gives rise to two terms that do not have a conventional diagrammatic representation, one of which we will refer to as the *perturbed orbital* (or PO term) and the other the *derivative* term. The perturbed orbital term, which has been treated in Ref. [4], is separately gauge invariant when covariant gauges are used (Feynman gauge is used in this calculation), as is the sum of the nested diagram, overlapping diagram, and derivative term. We treat only the latter set in the present paper.

As with the two-loop vacuum polarization diagram, the first two terms in the power series of the fourth-order self-energy are known [5,6] to be

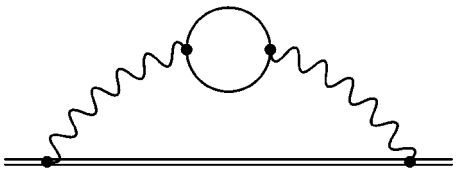

FIG. 1. Fourth-order vacuum polarization diagram.

$$E^{4SE}(Z\alpha)=[0.142\,787-2.15(5)(Z\alpha)](Z\alpha)^4 \text{ a.u.} \quad (2)$$

The remarkably large coefficient of the second term not only indicates the need for an evaluation to all orders of $Z\alpha$ at high $Z$, but also makes such a treatment desirable even for low $Z$.

While experiments that measure the ground-state Lamb shift in hydrogenlike uranium have reached the 16-eV level [7], far higher accuracies have been reached in the more easily measured spectra of highly charged many-electron ions. Particularly precise measurements have been made of the $2s_{1/2}$-$2p_{1/2}$ transition energy in lithiumlike uranium [9] and the $2s_{1/2}$-$2p_{3/2}$ transition energy in lithiumlike bismuth [10], the latter having been determined with an accuracy of 0.04 eV. Assuming $Z^4/n^3$ scaling, this would correspond to an accuracy of 0.48 eV in ground-state uranium. While the Lamb shift in a many-electron ion differs from the hydrogenic Lamb shift because of screening effects, the effect is relatively small, amounting to only a few percent, and can be neglected for the two-loop Lamb shift. However, the screening effect on the one-loop Lamb shift needs to be calculated along with two-photon exchange diagrams before the two-loop Lamb shift can be unambiguously isolated.

The lithiumlike bismuth experiment, when compared with the most complete calculation to date, that of Blundell [8], differs by 0.11 eV. The calculation takes account of the bulk of the screening effect, but leaves out two-photon exchange diagrams and keeps only the leading term of the two-loop Lamb shift. Unless the higher-order corrections to the two-loop Lamb shift cancel with the two-photon exchange terms, this indicates that the general size of the effects is on the order of a tenth of an eV. In this paper we will calculate several, though not all, contributions to the two-loop self-energy diagrams for the ground state. The size at $Z=83$ and $Z=92$ is generally of the order of 1 eV, which would scale to 0.125 eV for the $2s$ state, consistent with the above estimates. There is of course no substitute for a direct calculation of the two-loop Lamb shift, the subject of this paper.

A central issue in the exact evaluation of two-loop diagrams in the bound-state problem is the treatment of renormalization. In the one-loop case, the first calculations [11,12] subtracted a free Dirac propagator from the Dirac-Coulomb propagator, which allowed the isolation of the self-mass in-

 

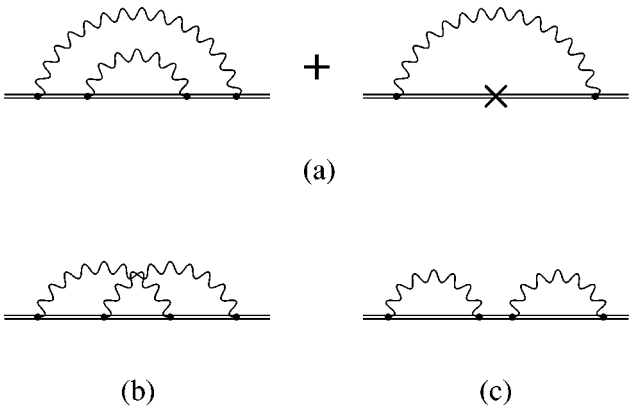


FIG. 2. Fourth-order self-energy diagrams.

finity, although great care had to be taken with other ultraviolet infinities not explicitly removed by this process, which however cancel because of the Ward identity. Mohr [13] and later Blundell and Snyderman [14] and Cheng *et al.* [15] carried out additional subtractions that allowed completely finite expressions to be dealt with. We note also the work of Lindgren *et al.* [16], which is known as partial wave renormalization. However, the situation is considerably more complicated when two loops are present. The source of the complication is subdivergences that lead to more severe ultraviolet divergences. When Pauli-Villars regularization is used, this leads to terms proportional to $\ln^2(\Lambda/m)$, and when dimensional regularization is used to terms proportional to $1/\epsilon^2$. One scheme to treat renormalization that works in the framework of partial wave renormalization has been presented in Ref. [17]; however, in this paper we have adopted a different approach based, as in the one-loop case, on subtracting diagrams with some Dirac-Coulomb propagators replaced with free propagators, which we refer to as zero-potential (0P) terms, or free propagators followed by an interaction with the nuclear Coulomb field followed by another free propagator, which we will refer to as 1P terms.

In the present paper we will present a treatment of the two-loop self-energy diagrams that divides into three parts. In the first part we deal with the unrenormalized diagrams, but make them ultraviolet finite by carrying out the kind of subtractions just described: we will refer to the unrenormalized diagrams together with the subtractions that make them finite as the $M$ term. This part of the calculation involves a double integral over Wick rotated photon energies and we carry it out in this paper for the experimentally interesting cases of $Z=92$ and $Z=83$. A complication in the evaluation of the $M$ term is the presence of reference-state singularities, which arise when intermediate states in the spectral decomposition of the electron propagators coincide with the valence state. We present a method of regularizing these singularities and show the mechanism for their cancellation.

In the next step of the calculation, the subtraction terms are Fourier transformed into momentum space. Some of them involve only free-electron propagators and can be evaluated with standard Feynman parameter techniques. However, other subtraction terms involve Dirac-Coulomb propagators. These latter terms are made ultraviolet finite by introducing a separate set of subtractions in which the remaining Dirac-Coulomb propagators are again replaced with 0P or 1P terms. The resulting ultraviolet finite quantity we denote as the $P$ term and defer its evaluation for a subsequent work, as it requires the development of new techniques for the treatment of the Dirac-Coulomb propagator in momentum space. Finally, the separate set of subtractions introduced to make the $P$ term ultraviolet finite can also be evaluated with Feynman parameter techniques. We group together the terms involving only free-electron propagators into the third part of the calculation, which we call the $F$ term. This part of the calculation, which is much less computationally intensive than the $M$ term, is carried out for a range of $Z$ values.

The plan of the paper is the following. The basic formulas for the unrenormalized two-loop diagrams are given in Sec. I along with one-loop formulas needed in the analysis. The subtraction scheme that defines the $M$ term is described in Sec. II and a discussion of reference-state singularities is given in Sec. III. Numerical results for the ground-state of hydrogenic uranium and bismuth are given in Sec. IV. The $P$ term is introduced in Sec. V, where the secondary subtraction terms that make it finite are introduced. The $F$ terms are evaluated in Sec. VI and although the calculation is still incomplete because the $P$ term has not been evaluated, the present numerical status of the fourth-order self-energy for hydrogenlike uranium is discussed at the end of that section. The issues that must be faced to complete the calculation are discussed in Sec. VII.

## I. BASIC FORMULAS

### A. One-loop self-energy and vertex functions

Before we evaluate the one-loop self-energy term, it is convenient for later use to define two one-loop operators regularized by working in $n=4-\epsilon$ dimensions. The first is the one-loop self-energy operator with a free-electron propagator in the Feynman gauge

$$\Sigma^{(2:0P)}(p)=-ie^2\int\frac{d^nk}{(2\pi)^n}\frac{1}{k^2+i\delta}\gamma_\mu\frac{1}{\not p-\not k-m}\gamma^\mu. \quad (3)$$

We define the ultraviolet finite part of this to be $\Sigma_c^{(2:0P)}(p)$ through

$$\Sigma^{(2:0P)}(p)=\delta m^{(2)}+\widetilde{B}^{(2)}(\not p-m)+\Sigma_c^{(2:0P)}(p). \quad (4)$$

Here

$$\delta m^{(2)}=\frac{m\alpha C}{2\pi\epsilon}\frac{3-\epsilon}{1-\epsilon} \quad (5)$$

and

$$\widetilde{B}^{(2)}=-\frac{\alpha C}{2\pi\epsilon}, \quad (6)$$

where $C=(4\pi)^{\epsilon/2}\Gamma(1+\epsilon/2)$. Note that we do not pull out the full wave function renormalization factor of $B^{(2)}$, but only the ultraviolet divergent part of it. The finite term is then

$$\Sigma_c^{(2:0P)}(p)=-\frac{\alpha C}{2\pi(1-\epsilon)}(\not p-m)+\frac{\alpha C}{4\pi}\left[\frac{p^2}{m^2}-1\right]\int_0^1 dx\left[m\frac{4-\epsilon}{1-\epsilon}-\not p\left(\frac{2-\epsilon}{1-\epsilon}-x\right)\right]\frac{x^{-\epsilon/2}}{[x-(p^2/m^2-1)(1-x)]^{1+\epsilon/2}}. \tag{7}$$

Note that we keep the exact $\epsilon$ dependence of this function, as it is necessary for use in the two-loop Lamb shift.

The second operator is the vertex function

$$\Lambda_\rho^{(2)}(p_2,p_1)=-ie^2\int\frac{d^nk}{(2\pi)^n}\frac{1}{k^2+i\delta}\gamma_\mu\times\frac{1}{\not k-\not p_2-m}\gamma_\rho\frac{1}{\not k-\not p_1-m}\gamma^\mu. \tag{8}$$

We again define a finite part through

$$\Lambda_\rho^{(2)}(p_2,p_1)=\tilde L^{(2)}\gamma_\rho+\Lambda_{c\rho}^{(2)}(p_2,p_1), \tag{9}$$

with

$$\tilde L^{(2)}=\frac{\alpha C}{2\pi\epsilon} \tag{10}$$

and

$$\Lambda_{c\rho}^{(2)}(p_2,p_1)=-\frac{\alpha C(4-\epsilon)}{8\pi}\gamma_\rho+\frac{\alpha C(2-\epsilon)^2}{4\pi\epsilon}\gamma_\rho\int_0^1\rho\,d\rho\int_0^1 dx\left[\frac{1}{\Delta^{\epsilon/2}}-1\right]-\frac{\alpha C}{4\pi}\int_0^1\rho\,d\rho\int_0^1 dx\frac{N_\rho}{\Delta^{1+\epsilon/2}}. \tag{11}$$

Again, we remark that $\tilde L^{(2)}$ is only the $1/\epsilon$ part of the vertex renormalization constant; however, the Ward identity $\tilde B^{(2)}=-\tilde L^{(2)}$ is still satisfied. We have introduced the functions

$$\Delta=\rho^2\epsilon_v^2-\rho^2|x\vec p_1+(1-x)\vec p_2|^2+\rho(m^2-\epsilon_v^2)+\rho x\vec p_1{}^2+\rho(1-x)\vec p_2{}^2, \tag{12}$$

where $\epsilon_v$ is the ground-state energy, and

$$N_\rho=\gamma_\mu\{-\rho x\not p_1+[1-\rho(1-x)]\not p_2+m\}\gamma_\rho[(1-\rho x)\not p_1-\rho(1-x)\not p_2+m]\gamma^\mu. \tag{13}$$

### B. One-loop Lamb shift

When we analyze the two-loop Lamb shift, expressions related to the one-loop Lamb shift frequently arise, so we review its treatment here. A novel feature is the need to evaluate the one-loop Lamb shift in $n$ dimensions. While when treated by itself the limit $n\to4$ can be taken after renormalization, we will find in the two-loop calculation certain terms in which the one-loop Lamb shift is multiplied by $1/\epsilon$. Thus we must keep order $\epsilon$ terms in order not to miss a finite contribution.

We begin by introducing the more general function

$$\Sigma_{mn}^{(2)}(E)\equiv-ie^2\int d^3x\;d^3y\int\frac{d^nk}{(2\pi)^n}\frac{e^{i\vec k\cdot(\vec x-\vec y)}}{k^2+i\delta}\times\overline{\psi_m}(\vec x)\gamma_\mu S_F(\vec x,\vec y;E-k_0)\gamma^\mu\psi_n(\vec y). \tag{14}$$

In terms of this function, the energy shift of a state $v$ associated with the one-loop self-energy is $\Sigma_{vv}^{(2)}(\epsilon_v)$, which for notational simplicity will be denoted $\Sigma^{(2)}$ in the following. It is to be distinguished from the operator $\Sigma^{(2)}(p)$ introduced in Sec. I A. As will also be the case for the two-loop calculation, we adopt the approach of working with unrenormalized diagrams, carrying out renormalization by introducing counterterms explicitly. Thus this diagram will contain the self-mass infinity as well as canceling vertex and wave function infinities. To isolate these terms, we make the standard expansion of the bound electron propagator in terms of the free electron propagator $S_F^0$,

$$S_F(\mathbf{r},\mathbf{r}';E)=S_F^0(\mathbf{r},\mathbf{r}';E)+\int d^3x\;S_F^0(\mathbf{r},\mathbf{x};E)\gamma_0V(\mathbf{x})S_F^0(\mathbf{x},\mathbf{r}';E)+\int d^3x\;d^3y\;S_F^0(\mathbf{r},\mathbf{x};E)\gamma_0V(\mathbf{x})\times S_F(\mathbf{x},\mathbf{y};E)\gamma_0V(\mathbf{y})S_F^0(\mathbf{y},\mathbf{r}';E), \tag{15}$$

where for this calculation $V(\mathbf{x})$ is taken to be the Coulomb potential. Insertion of the first two terms on the right-hand side in Eq. (14) gives the 0P and 1P terms and insertion of the last the many-potential (MP) term. The 0P and 1P terms can be obtained as the expectation values of the functions introduced in Sec. I A. The 0P term is

$$\Sigma^{(2:0P)}=\delta m^{(2)}\int d^3p\;\overline{\psi_v}(\vec p)\psi_v(\vec p)+\tilde B^{(2)}\int d^3p\;\overline{\psi_v}(\vec p)(\not p-m)\psi_v(\vec p)+C\Sigma_c^{(2:0P)}. \tag{16}$$

Here we have explicitly removed the constant $C$ from the definition of $\Sigma_c^{(2:0P)}$.

In the $n\to4$ limit, a straightforward analysis [15] gives

$$\Sigma_{c,4}^{(2:0P)}=-\frac{\alpha}{2\pi}\int d^3p\ \overline{\psi_v}(\vec{p})(\not{p}-m)\psi_v(\vec{p})$$
$$+\frac{\alpha}{2\pi}\int d^3p\left[\frac{p^2}{m^2}-1\right]$$
$$\times\int_0^1 dx\frac{\overline{\psi_v}(\vec{p})[2m-\not{p}\ (1-x/2)]\psi_v(\vec{p})}{x-(p^2/m^2-1)(1-x)}. \quad (17)$$

Here the subscript $c,4$ indicates that $n=4$; expressions with the subscript $c$ by itself are understood to be evaluated in $n$ dimensions.

Similarly, we write

$$\Sigma^{(2:1P)}=\tilde{L}^{(2)}\int d^3p\ \overline{\psi_v}(\vec{p})(\not{p}-m)\psi_v(\vec{p})+C\Sigma_c^{(2:1P)} \quad (18)$$

where in the limit $n\to 4$

$$\Sigma_{c,4}^{(2:1P)}=-\frac{\alpha}{2\pi}\int d^3p\ \overline{\psi_v}(\vec{p})(\not{p}-m)\psi_v(\vec{p})$$
$$+\frac{Z\alpha^2}{8\pi^3}\int_0^1\rho\ d\rho\int_0^1 dx\int\frac{d^3p_1d^3p_2}{|\vec{p}_1-\vec{p}_2|^2}\frac{N}{\Delta}$$
$$+\frac{Z\alpha^2}{4\pi^3}\int_0^1\rho\ d\rho\int_0^1 dx\int\frac{d^3p_1d^3p_2}{|\vec{p}_1-\vec{p}_2|^2}$$
$$\times\overline{\psi_v}(\vec{p}_2)\gamma_0\psi_v(\vec{p}_1)\ln\frac{\Delta}{m^2}. \quad (19)$$

Here $N\equiv\overline{\psi_v}(p_2)N_{\rho=0}\psi_v(p_1)$, where $N_\rho$ and $\Delta$ are given in Sec. I A. The MP term is ultraviolet finite. After including the self-mass counterterm and noting the cancellation of the remaining divergences, we have the finite result, to order $\epsilon$,

$$\Sigma_c^{(2)}=C[\Sigma_{c,4}^{(2:0P)}+\Sigma_{c,4}^{(2:1P)}+\Sigma_c^{(2:MP)}+\epsilon\Sigma_{c,\epsilon}^{(2:0P)}+\epsilon\Sigma_{c,\epsilon}^{(2:1P)}]. \quad (20)$$

The subscript $\epsilon$ indicate the terms of order $\epsilon$ in a Taylor expansion of $\Sigma_c^{(2:0P)}$ and $\Sigma_c^{(2:1P)}$.

For the one-loop Lamb shift, one can take $n\to 4$, and this reduces to

$$\Sigma_{c,4}^{(2)}=\Sigma_{c,4}^{(2:0P)}+\Sigma_{c,4}^{(2:1P)}+\Sigma_{c,4}^{(2:MP)}. \quad (21)$$

However, as mentioned above, we will encounter in the following expressions in which the exact one-loop Lamb shift is multiplied by $1/\epsilon$. While we will show that terms that involve the many-potential term cancel exactly, terms involving the zero- and one-potential terms cancel only the $n=4$ parts of these terms, leaving a finite contribution involving $\Sigma_{c,\epsilon}^{(2:0P)}$ and $\Sigma_{c,\epsilon}^{(2:1P)}$, which will be included in Sec. VI B.

### C. Two-loop self-energy

The basic expressions for the two-loop Lamb shift were given in Ref. [18]. The energy shift associated with the nested diagram is given by

$$\Sigma^{4N}=-e^4\int d^3x_1d^3x_2d^3x_3d^3x_4\int\frac{d^nk}{(2\pi)^n}\frac{d^nl}{(2\pi)^n}$$
$$\times\frac{e^{i\vec{k}\cdot(\vec{x}_1-\vec{x}_4)}}{k^2+i\delta}\frac{e^{i\vec{l}\cdot(\vec{x}_2-\vec{x}_3)}}{l^2+i\delta}\overline{\psi_v}(\vec{x}_1)\gamma^\mu$$
$$\times S_F(\vec{x}_1,\vec{x}_2;\epsilon_v-k_0)\gamma^\nu S_F(\vec{x}_2,\vec{x}_3;\epsilon_v-k_0-l_0)\gamma_\nu$$
$$\times S_F(\vec{x}_3,\vec{x}_4;\epsilon_v-k_0)\gamma_\mu\psi_v(\vec{x}_4). \quad (22)$$

It should be understood that this is always accompanied by the counterterm diagram

$$\Sigma_{\delta m}^{4N}=ie^2\int d^3x_1d^3x_2d^3x_3\int\frac{d^nk}{(2\pi)^n}\frac{e^{i\vec{k}\cdot(\vec{x}_1-\vec{x}_3)}}{k^2+i\delta}$$
$$\times\overline{\psi_v}(\vec{x}_1)\gamma^\mu S_F(\vec{x}_1,\vec{x}_2;\epsilon_v-k_0)\delta m^{(2)}$$
$$\times S_F(\vec{x}_2,\vec{x}_3;\epsilon_v-k_0)\gamma_\mu\psi_v(\vec{x}_3). \quad (23)$$

The overlapping diagram gives the energy shift

$$\Sigma^{4O}=-e^4\int d^3x_1d^3x_2d^3x_3d^3x_4\int\frac{d^nk}{(2\pi)^n}\frac{d^nl}{(2\pi)^n}$$
$$\times\frac{e^{i\vec{k}\cdot(\vec{x}_1-\vec{x}_3)}}{k^2+i\delta}\frac{e^{i\vec{l}\cdot(\vec{x}_2-\vec{x}_4)}}{l^2+i\delta}\overline{\psi_v}(\vec{x}_1)\gamma^\mu$$
$$\times S_F(\vec{x}_1,\vec{x}_2;\epsilon_v-k_0)\gamma^\nu S_F(\vec{x}_2,\vec{x}_3;\epsilon_v-k_0-l_0)\gamma_\mu$$
$$\times S_F(\vec{x}_3,\vec{x}_4;\epsilon_v-l_0)\gamma_\nu\psi_v(\vec{x}_4). \quad (24)$$

The perturbed orbital contribution is given by

$$\Sigma_{PO}=\sum_{n\neq v}\frac{\Sigma_{vn}(\epsilon_v)\Sigma_{nv}(\epsilon_v)}{\epsilon_v-\epsilon_n}. \quad (25)$$

If a perturbed orbital $\tilde{v}$ is defined through

$$|\tilde{v}\rangle\equiv\sum_{n\neq v}\frac{|n\rangle\Sigma_{nv}(\epsilon_v)}{\epsilon_v-\epsilon_n}, \quad (26)$$

the perturbed orbital term is simply $\Sigma_{v\tilde{v}}(\epsilon_v)$. Finally, the derivative term, which is again related to the one-loop self-energy, but in this case accounting for the shift in the energy flowing through the electron propagator from the one-loop Lamb shift, is given by

$$\Sigma^D=\Sigma_c^{(2)}\frac{\partial\Sigma_{vv}^{(2)}(E)}{\partial E}\Big|_{E=\epsilon_v}, \quad (27)$$

which more explicitly is

$$\Sigma^D=ie^2\Sigma_c^{(2)}\int d^3x\ d^3y\ d^3w\int\frac{d^nk}{(2\pi)^n}\frac{e^{i\vec{k}\cdot(\vec{x}-\vec{y})}}{k^2+i\delta}$$
$$\times\overline{\psi_v}(\vec{x})\gamma_\mu S_F(\vec{x},\vec{w};\epsilon_v-k_0)\gamma_0$$
$$\times S_F(\vec{w},\vec{y};\epsilon_v-k_0)\gamma^\mu\psi_v(\vec{y}). \quad (28)$$

Note that we have implicitly included the self-mass counterterm diagram, so that the finite part of the self-energy multiplies the derivative.

In this paper we are concerned with the sum of the nested diagram, overlapping diagram, and derivative term,

$$\Sigma^{4SE} \equiv \Sigma^{4N} + \Sigma^{4O} + \Sigma^{D}. \tag{29}$$

This accounts for all of the first term in the power series expansion given in Eq. (2) and some of the second term, with the remainder of the order $(Z\alpha)^5$ a.u. contribution coming from the PO term [4]. While in the present paper we are concerned only with the high-$Z$ case, in future work at low $Z$, a comparison with the known power series will both provide a check of the calculation and allow the isolation of new terms starting in order $(Z\alpha)^6$ a.u.

We record for later use the momentum space form of the nested and overlapping diagrams

$$\begin{aligned}\Sigma^{4N} = & -e^4 \int d^3p_2 d^3q_2 d^3q_1 d^3p_1 \int \frac{d^nk}{(2\pi)^n} \frac{d^nl}{(2\pi)^n} \\ & \times \frac{1}{k^2+i\delta} \frac{1}{l^2+i\delta} \overline{\psi_v}(\vec{p}_2)\gamma^\mu S_F(\vec{p}_2-\vec{k},\vec{q}_2-\vec{k};\epsilon_v-k_0) \\ & \times \gamma^\nu S_F(\vec{q}_2-\vec{k}-\vec{l},\vec{q}_1-\vec{k}-\vec{l};\epsilon_v-k_0-l_0) \\ & \times \gamma_\nu S_F(\vec{q}_1-\vec{k},\vec{p}_1-\vec{k};\epsilon_v-k_0)\gamma_\mu \psi_v(\vec{p}_1)\end{aligned} \tag{30}$$

and

$$\begin{aligned}\Sigma^{4O} = & -e^4 \int d^3p_2 d^3q_2 d^3q_1 d^3p_1 \int \frac{d^nk}{(2\pi)^n} \frac{d^nl}{(2\pi)^n} \\ & \times \frac{1}{k^2+i\delta} \frac{1}{l^2+i\delta} \overline{\psi_v}(\vec{p}_2)\gamma^\mu S_F(\vec{p}_2-\vec{k},\vec{q}_2-\vec{k};\epsilon_v-k_0) \\ & \times \gamma^\nu S_F(\vec{q}_2-\vec{k}-\vec{l},\vec{q}_1-\vec{k}-\vec{l};\epsilon_v-k_0-l_0) \\ & \times \gamma_\mu S_F(\vec{q}_1-\vec{l},\vec{p}_1-\vec{l};\epsilon_v-l_0)\gamma_\nu \psi_v(\vec{p}_1).\end{aligned} \tag{31}$$

Were it not for the ultraviolet divergences present in these expressions, their exact evaluation would be straightforward using the partial wave decomposition of the electron and photon propagators in coordinate space. Specifically, we can express the electron propagators as

$$\begin{aligned}S_F(\vec{y},\vec{z};E) = \sum_{\kappa,\mu} [ & \theta(y-z) w^E_{\kappa\mu}(\vec{y})\, \overline{u^E_{\kappa\mu}}(\vec{z}) \\ & + \theta(z-y) u^E_{\kappa\mu}(\vec{y})\, \overline{w^E_{\kappa\mu}}(\vec{z})],\end{aligned} \tag{32}$$

where $w^E_{\kappa\mu}, u^E_{\kappa\mu}$ are the solutions of the Dirac equation with (in general complex) energy $E$ regular at infinity and the origin, respectively (defined to include a Wronskian factor), which have the representation

$$u^E_{\kappa\mu}(\vec{r}) = \frac{1}{r} \begin{Bmatrix} i g_0^{\kappa,E}(r)\chi_{\kappa\mu}(\hat{r}) \\ f_0^{\kappa,E}(r)\chi_{-\kappa\mu}(\hat{r}) \end{Bmatrix} \tag{33}$$

and

$$w^E_{\kappa\mu}(\vec{r}) = \frac{1}{r} \begin{Bmatrix} i g_\infty^{\kappa,E}(r)\chi_{\kappa\mu}(\hat{r}) \\ f_\infty^{\kappa,E}(r)\chi_{-\kappa\mu}(\hat{r}) \end{Bmatrix}. \tag{34}$$

Here $g_0^{\kappa,E}, f_0^{\kappa,E}$ are the radial wave functions regular at the origin, $g_\infty^{\kappa,E}, f_\infty^{\kappa,E}$ the radial wave functions regular at infinity, and $\chi_{\kappa\mu}$ spherical spinors. After putting this form into the above equations along with the standard representation of the photon propagator in terms of spherical Bessel functions, the angle integrations can be carried out analytically along with the summations over magnetic quantum numbers. The presence of the $\theta$ functions requires a division of the radial integrations over the four variables into 24 regions, corresponding to the 24 orderings in relative magnitude of these variables. For brevity, we show below only one ordering $|\vec{x}_1| \geq |\vec{x}_2| \geq |\vec{x}_3| \geq |\vec{x}_4|$, which we refer to as region I, and also give only the expression for the case $\mu=0, \nu=0$. We define the function

$$R_{ij}(x;E_i,E_j) \equiv g_i(x)g_j(x) + f_i(x)f_j(x), \tag{35}$$

where $E_i$ is the energy associated with the Dirac equation that $g_i, f_i$ solve, and similarly for $E_j$. Then the ordering above, with $\mu$ and $\nu$ restricted to being timelike, gives the integrals

$$\begin{aligned}\Sigma^{4N}(I) = & \frac{\alpha^2}{2\pi^2} \sum_{\kappa_1,\kappa_2,\kappa_3,l_1,l_2}^{\kappa_3=\kappa_1} \frac{(2l_1+1)(2l_2+1)}{(2j_v+1)(2j_{\kappa_1}+1)} \\ & \times (-1)^{l_1+l_2+j_v+j_{\kappa_2}} C^2_{l_1}(\kappa_v\kappa_1) C^2_{l_2}(\kappa_1\kappa_2) \\ & \times \int_{-\infty}^{\infty} k_0 dk_0 \int_{-\infty}^{\infty} l_0 dl_0 \int_0^{\infty} dx_1 \int_0^{x_1} dx_2 \int_0^{x_2} dx_3 \\ & \times \int_0^{x_3} dx_4 j_{l_1}(k_0x_4) h^{(1)}_{l_1}(k_0x_1) j_{l_2}(l_0x_3) h^{(1)}_{l_2}(l_0x_2) \\ & \times R_{v\infty_1}(x_1;\epsilon_v,\epsilon_v-k_0) R_{0_1\infty_2}(x_2;\epsilon_v-k_0,\epsilon_v-k_0-l_0) \\ & \times R_{0_2\infty_3}(x_3,\epsilon_v-k_0-l_0,\epsilon_v-k_0) R_{0_3v}(x_4;\epsilon_v-k_0,\epsilon_v)\end{aligned} \tag{36}$$

and

$$\begin{aligned}\Sigma^{4O}(I) = & -\frac{\alpha^2}{2\pi^2} \sum_{\kappa_1,\kappa_2,\kappa_3,l_1,l_2} \frac{(2l_1+1)(2l_2+1)}{(2j_v+1)} \\ & \times (-1)^{l_1+l_2+j_v+j_{\kappa_1}+j_{\kappa_2}+j_{\kappa_3}} C_{l_1}(\kappa_v\kappa_1) \\ & \times C_{l_1}(\kappa_2\kappa_3) C_{l_2}(\kappa_1\kappa_2) C_{l_2}(\kappa_3\kappa_v) \\ & \times \begin{Bmatrix} j_{\kappa_1} & l_1 & j_v \\ j_{\kappa_3} & l_2 & j_{\kappa_2} \end{Bmatrix} \int_{-\infty}^{\infty} k_0 dk_0 \int_{-\infty}^{\infty} l_0 dl_0 \int_0^{\infty} dx_1 \\ & \times \int_0^{x_1} dx_2 \int_0^{x_2} dx_3 \int_0^{x_3} dx_4 \; j_{l_1}(k_0x_3) h^{(1)}_{l_1}(k_0x_1) \\ & \times j_{l_2}(l_0x_4) h^{(1)}_{l_2}(l_0x_2) R_{v\infty_1}(x_1;\epsilon_v,\epsilon_v-k_0) \\ & \times R_{0_1\infty_2}(x_2;\epsilon_v-k_0,\epsilon_v-k_0-l_0) \\ & \times R_{0_2\infty_3}(x_3;\epsilon_v-k_0-l_0,\epsilon_v-l_0) \\ & \times R_{0_3v}(x_4;\epsilon_v-l_0,\epsilon_v).\end{aligned} \tag{37}$$

Here

$$C_l(\kappa_i\kappa_j)\equiv(-1)^{j_i+1/2}\sqrt{(2j_i+1)(2j_j+1)}$$
$$\times\begin{Bmatrix} j_i & j_j & l \\ \frac{1}{2} & -\frac{1}{2} & 0 \end{Bmatrix}\Pi(l_i,l_j,l), \qquad (38)$$

where $\Pi(l_i,l_j,l)$ is a parity factor that vanishes unless the sum $l_i+l_j+l$ is even, in which case it is unity. Removal of the restriction $\mu=\nu=0$ leads to additional terms, formulas for which can be found in Ref. [19]. All of these expressions have ultraviolet infinities and we now describe a subtraction scheme to isolate and cancel these infinities.

## II. SUBTRACTION SCHEME

### A. Nested term

As with the one-loop self energy, our basic strategy for dealing with ultraviolet divergences is to introduce subtractions involving the free-electron propagator, which is far simpler than the full Dirac-Coulomb propagator, but which has the same ultraviolet behavior. In the case of the nested diagram, the subtraction scheme used here is to treat the interior electron propagator in the same fashion as in the one-loop self-energy, leaving, however, the outer electron propagators unchanged. We thus define the nested $M$ term as

$$\Sigma_M^N=-e^4\int d^3x_1d^3x_2d^3x_3d^3x_4$$
$$\times\int\frac{d^nk}{(2\pi)^n}\frac{d^nl}{(2\pi)^n}\frac{e^{i\vec{k}\cdot(\vec{x}_1-\vec{x}_4)}}{k^2+i\delta}\frac{e^{i\vec{l}\cdot(\vec{x}_2-\vec{x}_3)}}{l^2+i\delta}$$
$$\times\overline{\psi_v}(\vec{x}_1)\gamma^\mu S_F(\vec{x}_1,\vec{x}_2;\epsilon_v-k_0)$$
$$\times\gamma^\nu[S_F(\vec{x}_2,\vec{x}_3;\epsilon_v-k_0-l_0)-S_0(\vec{x}_2,\vec{x}_3;\epsilon_v-k_0-l_0)$$
$$-S_1(\vec{x}_2,\vec{x}_3;\epsilon_v-k_0-l_0)]$$
$$\times\gamma_\nu S_F(\vec{x}_3,\vec{x}_4;\epsilon_v-k_0)\gamma_\mu\psi_v(\vec{x}_4)$$
$$\equiv\Sigma^{4N}-\Sigma^{N1}-\Sigma^{N2}. \qquad (39)$$

Here

$$S_1(\vec{x},\vec{y};\epsilon)\equiv-\int d^3z\,S_0(\vec{x},\vec{z};\epsilon)\frac{Z\alpha\gamma_0}{|\vec{z}|}S_0(\vec{z},\vec{y};\epsilon). \qquad (40)$$

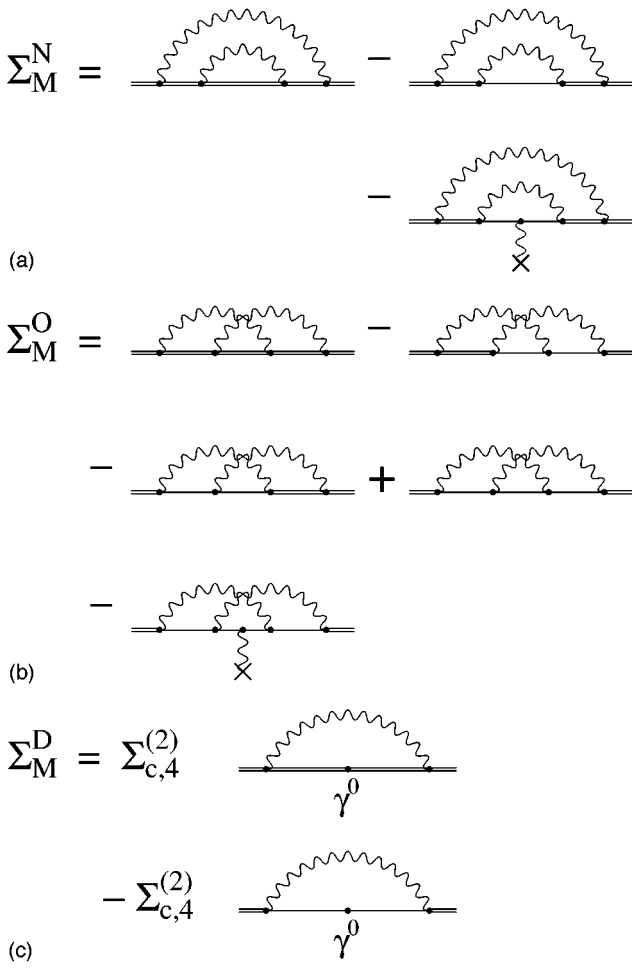


FIG. 3. Diagrammatic representation of the subtraction scheme that defines the $M$ term.

As with $\Sigma^{4N}$, $\Sigma^{N1}$ is understood to be accompanied by the counterterm diagram $\Sigma^{4N}_{\delta m}$. The diagrammatic expression of this is shown in Fig. 3(a). Standard power counting arguments show that $\Sigma^{4N}_M$ is ultraviolet finite.

### B. Overlap term

The subtractions necessary to render the overlapping diagram finite are somewhat more complicated than the nested diagram. In this case, while it is possible to devise a subtraction in which only the center electron propagator is bound, the resulting expression would be difficult to analyze since it would involve ultraviolet-divergent subdiagrams in which one propagator was free and the other bound. Instead, we first subtract terms in which the leftmost two or rightmost two propagators are free. This oversubtracts the leading divergence, in which all propagators are free, so we add that term back in. Since this subtraction scheme misses a divergent term in which the middle propagator has an interaction, we finally subtract that term with the outer propagators free. The overlapping $M$ term has the explicit representation

$$\Sigma_M^O = -e^4 \int d^3x_1 d^3x_2 d^3x_3 d^3x_4 \int \frac{d^nk}{(2\pi)^n} \frac{d^nl}{(2\pi)^n} \frac{e^{i\vec{k}\cdot(\vec{x}_1-\vec{x}_3)}}{k^2+i\delta} \frac{e^{i\vec{q}\cdot(\vec{x}_2-\vec{x}_4)}}{l^2+i\delta} \overline{\psi_v}(\vec{x}_1)\gamma_\mu [S_F(\vec{x}_1,\vec{x}_2;\epsilon_v-k_0)\gamma^\nu$$
$$\times S_F(\vec{x}_2,\vec{x}_3;\epsilon_v-k_0-l_0)\gamma^\mu S_F(\vec{x}_3,\vec{x}_4;\epsilon_v-l_0) - S_F(\vec{x}_1,\vec{x}_2;\epsilon_v-k_0)\gamma^\nu S_0(\vec{x}_2,\vec{x}_3;\epsilon_v-k_0-l_0)\gamma^\mu S_0(\vec{x}_3,\vec{x}_4;\epsilon_v-l_0)$$
$$- S_0(\vec{x}_1,\vec{x}_2;\epsilon_v-k_0)\gamma^\nu S_0(\vec{x}_2,\vec{x}_3;\epsilon_v-k_0-l_0)\gamma^\mu S_F(\vec{x}_3,\vec{x}_4;\epsilon_v-l_0) + S_0(\vec{x}_1,\vec{x}_2;\epsilon_v-k_0)\gamma^\nu$$
$$\times S_0(\vec{x}_2,\vec{x}_3;\epsilon_v-k_0-l_0)\gamma^\mu S_0(\vec{x}_3,\vec{x}_4;\epsilon_v-l_0) - S_0(\vec{x}_1,\vec{x}_2;\epsilon_v-k_0)\gamma^\nu S_1(\vec{x}_2,\vec{x}_3;\epsilon_v-k_0-l_0)\gamma^\mu$$
$$\times S_0(\vec{x}_3,\vec{x}_4;\epsilon_v-l_0)]\gamma_\nu\psi_v(\vec{x}_4)$$
$$\equiv \Sigma^{4O} - \Sigma^{O1} - \Sigma^{O2} + \Sigma^{O3} - \Sigma^{O4}. \tag{41}$$

Again, power counting arguments show the overlapping $M$ term is ultraviolet finite. The diagrams representing the subtraction are shown in Fig. 3(b).

### C. Derivative term

We now turn to an analysis of $\Sigma^D$. We note that this same expression is encountered when considering the effect of external potentials on radiative corrections, recently considered in Ref. [19]. The ultraviolet divergence of this term will play an important role in combination with the nested and overlapping diagrams. To isolate it we subtract from the diagram a similar term with both electron propagators replaced with free propagators. The derivative $M$ term $\Sigma_M^D$ is given by

$$\Sigma_M^D = ie^2\Sigma_{c,4}^{(2)} \int d^3x\ d^3y\ d^3w$$
$$\times \int \frac{d^nk}{(2\pi)^n} \frac{e^{i\vec{k}\cdot(\vec{x}-\vec{y})}}{k^2+i\delta} \overline{\psi_v}(\vec{x})\gamma_\mu [S_F(\vec{x},\vec{w};\epsilon_v-k_0)$$
$$\times \gamma_0 S_F(\vec{w},\vec{y};\epsilon_v-k_0) - S_0(\vec{x},\vec{w};\epsilon_v-k_0)$$
$$\times \gamma_0 S_0(\vec{w},\vec{y};\epsilon_v-k_0)]\gamma^\mu\psi_v(\vec{y})$$
$$\equiv \Sigma^{4D} - \Sigma^{D1}. \tag{42}$$

This is represented diagrammatically in Fig. 3(c). We have replaced $\Sigma_c^{(2)}$ with its $n\to 4$ limit since it multiplies an ultraviolet finite expression. The $M$ term is then

$$\Sigma_M = \Sigma_M^N + \Sigma_M^O + \Sigma_M^D. \tag{43}$$

While ultraviolet finite, it contains reference-state singularities, which we now discuss.

## III. REFERENCE-STATE SINGULARITIES

Reference-state singularities can occur in bound-state QED calculations when the intermediate states in the spectral decomposition of the electron propagators coincide with the valence state. We regulate them by altering the valence energy to $\epsilon_v' \equiv \epsilon_v(1-\Delta)$ in the electron Green's functions. This regulator is described in Refs. [19,20]. As an example of a reference-state singularity we consider the first term in $\Sigma_M^D$. Representing the electron propagators with spectral decompositions, this term becomes

$$\Sigma^D = ie^2\Sigma_{c,4}^{(2)} \sum_m \sum_n \int d^3x\ d^3y\ d^3w$$
$$\times \int \frac{d^nk}{(2\pi)^n} \frac{e^{i\vec{k}\cdot(\vec{x}-\vec{y})}}{k^2+i\delta}$$
$$\times \frac{\overline{\psi_v}(\vec{x})\gamma_\mu\psi_m(\vec{x})\,\overline{\psi_m}(\vec{w})\gamma_0\psi_n(\vec{w})\,\overline{\psi_n}(\vec{y})\gamma^\mu\psi_v(\vec{y})}{[\epsilon_v'-k_0-\epsilon_m(1-i\delta)][\epsilon_v'-k_0-\epsilon_n(1-i\delta)]}. \tag{44}$$

Restricting the sum to $\epsilon_m=\epsilon_v$, $\epsilon_n=\epsilon_v$ and taking $n\to 4$ gives

$$\Sigma_{\rm ref}^D = ie^2\Sigma_{c,4}^{(2)} \sum_{m_a} \sum_{m_b} \int d^3x\ d^3y\ d^3w \int \frac{d^4k}{(2\pi)^4} \frac{e^{i\vec{k}\cdot(\vec{x}-\vec{y})}}{k^2+i\delta}$$
$$\times \frac{\overline{\psi_v}(\vec{x})\gamma_\mu\psi_a(\vec{x})\,\overline{\psi_a}(\vec{w})\gamma_0\psi_b(\vec{w})\,\overline{\psi_b}(\vec{y})\gamma^\mu\psi_v(\vec{y})}{[\epsilon_v'-k_0-\epsilon_v+i\delta]^2}, \tag{45}$$

where $a$ represents a valence state with magnetic quantum number $m_a$ and $b$ a valence state with magnetic quantum number $m_b$. The $d^3w$ integration can be carried out to give

$$\Sigma_{\rm ref}^D = ie^2\Sigma_{c,4}^{(2)} \sum_{m_a} \int d^3x\ d^3y \int \frac{d^4k}{(2\pi)^4}$$
$$\times \frac{e^{i\vec{k}\cdot(\vec{x}-\vec{y})}}{k^2+i\delta} \frac{\overline{\psi_v}(\vec{x})\gamma_\mu\psi_a(\vec{x})\,\overline{\psi_a}(\vec{y})\gamma^\mu\psi_v(\vec{y})}{[\epsilon_v'-k_0-\epsilon_v+i\delta]^2}. \tag{46}$$

Without the regulator this would appear to lead to a linear divergence at $k_0=0$. As discussed in more detail in Ref. [19], the term would actually vanish by Cauchy's theorem were it not for the $k_0$ dependence of the photon propagator. That dependence leads to a logarithmic singularity, which can be shown to be

$$\Sigma^D_{\rm ref}({\rm singular}) = -\frac{\alpha}{\pi}\ln\Delta\ \Sigma^{(2)}_{c,4}. \tag{47}$$

While we will show that this singularity cancels against a term from the nested diagram, we choose here to carry out a numerical fit. Specifically, by using successively smaller values of $\Delta$, a fit to the form

$$\Sigma^D_M = \frac{\alpha}{\pi}\Sigma^{(2)}_{c,4}[-\ln\Delta + A + B\Delta] \tag{48}$$

allows an accurate determination of the constant $A$.

We now show that this reference-state singularity cancels with another reference-state singularity associated with the nested term. To do this, we treat the first and last electron propagators in Eqs. (22) and (23) in the same way as with the derivative term, in addition changing the energy in the intermediate propagator to $\epsilon'_v$, which gives the expression

$$\Sigma^{4N}_{\rm ref} = -ie^2\sum_{m_a,m_b}\int d^3x_1 d^3x_4 \int \frac{d^4k}{(2\pi)^n}\frac{e^{i\vec{k}\cdot(\vec{x}_1-\vec{x}_4)}}{k^2+i\delta} \times \frac{\overline{\psi_v}(\vec{x}_1)\gamma^\mu\psi_a(\vec{x}_1)\Sigma^{(2)}_{ab}(\epsilon'_v-k_0)\overline{\psi_b}(\vec{x}_4)\gamma_\mu\psi_v(\vec{x}_4)}{[\epsilon'_v-k_0-\epsilon_v+i\delta]^2}, \tag{49}$$

where we have used Eq. (14). Note that the self-mass counterterm is understood to be subtracted from $\Sigma^{(2)}_{ab}$. In the limit $k_0\to 0,\Delta\to 0$, we can replace $\Sigma^{(2)}_{ab}(\epsilon'_v-k_0)$ with $\Sigma^{(2)}_{c,4}\delta_{m_a m_b}$ and the integrands of the derivative term and nested term can be seen to cancel.

If we were including only the unsubtracted derivative and nested diagrams, the above argument shows the complete cancellation of the reference-state singularities. However, our subtraction scheme is equivalent to replacing $\Sigma^{(2)}_{wx}(\epsilon'_v-k_0)$ with $\Sigma^{(2:MP)}_{wx}(\epsilon'_v-k_0)$ in Eq. (49). For this reason the $M$ terms have a reference-state singularity proportional to $\Sigma^{(2:0P)}_{c,4}+\Sigma^{(2:1P)}_{c,4}$ that will be canceled by a corresponding singularity in the $P$ term. The occurrence of this singularity, which will be shown below, provides one of the checks of the calculation.

## IV. NUMERICAL EVALUATION OF THE $M$ TERMS

At this point the ultraviolet finite expressions for the $M$ terms are ready for numerical evaluation. We begin with the derivative term. Its angular reduction, details of which are given in Ref. [19], involves a single sum over a photon angular momentum $l$. We carry out the sum up to $l=12$, at which point the behavior is almost exactly $1/l^3$, which allows the sum to infinity to be carried out. The reference-state singularity occurs only for $l=0$ and is treated as described above. The final result for this term is

$$\Sigma^D_M = -\frac{\alpha}{\pi}\Sigma^{(2)}_{c,4}\ \ln\Delta + \begin{cases} -0.033\,95 & \text{a.u.}, \quad Z=83 \\ -0.043\,98 & \text{a.u.}, \quad Z=92. \end{cases} \tag{50}$$

We next consider the overlapping $M$ term, which does not have any reference-state singularities. However, we still retain the regulator. The reason for this is to avoid poles and cuts in the complex energy plane when we Wick rotate the variables $k_0$ and $l_0$ to the imaginary axis. It is useful to recall the situation with the one-loop self-energy. In this case, after performing subtractions to eliminate ultraviolet divergences, one Wick rotates $k_0\to i\omega_k$. However, the spectral decomposition of the electron propagator has a term with a denominator $1/(-k_0+i\delta)$. In this case a semicircle must be made around this pole, which gives rise to a contribution called the pole term, which plays an important numerical role in the Lamb shift. However, the regulator we have introduced to make the reference-state singularities finite moves this pole into the second quadrant, which eliminates the pole term. However, the price of this simplification is the need to put a larger number of integration points near the origin, as there is now additional structure at small $\omega_k$. Also, the calculation must be done for at least two values of the regulator and a linear fit performed to obtain the intercept.

The same considerations simplify both the overlapping and nested diagrams. By using the regulator, we can simply Wick rotate both $k_0\to i\omega_k$ and $l_0\to i\omega_l$. Without the regulator, several extra terms analogous to the pole term of the one-loop self-energy would be present. Because we include it, however, only the Wick rotated part of the calculation need be considered. However, as with the one-loop Lamb shift, care must be taken to include sufficient points at small $\omega_k$ and $\omega_l$ to accurately account for the structure in that region.

While in the one-loop Lamb shift the integral from $\omega_k=-\infty$ to 0 can be combined with the integral from $\omega_k=0$ to $\infty$, in the two-loop Lamb shift the four regions can be reduced to only two. Specifically, the $\omega_k=-\infty,\ldots,0,\omega_l=-\infty,\ldots,0$ region combines with the $\omega_k=0,\ldots,\infty,\omega_l=0,\ldots,\infty$ region and the $\omega_k=-\infty,\ldots,0,\omega_l=0,\ldots,\infty$ region combines with the $\omega_k=0,\ldots,\infty,\omega_l=-\infty,\ldots,0$ region. For the overlapping diagram, there then results for region $I$, with $x_1>x_2>x_3>x_4$, and again showing only the $\mu=\nu=0$ contribution,

$$\Sigma^{4O}(I)=-\frac{\alpha^2}{2\pi^2}\sum_{\kappa_{123},l_{12}}\frac{(2l_1+1)(2l_2+1)}{(2j_v+1)}(-1)^{l_1+l_2+j_v+j_{\kappa_1}+j_{\kappa_2}+j_{\kappa_3}}C_{l_1}(\kappa_v\kappa_1)C_{l_1}(\kappa_2\kappa_3)C_{l_2}(\kappa_1\kappa_2)C_{l_2}(\kappa_3\kappa_v)$$
$$\times\begin{Bmatrix} j_{\kappa_1} & l_1 & j_v \\ j_{\kappa_3} & l_2 & j_{\kappa_2}\end{Bmatrix}\int_0^\infty\omega_k d\omega_k\int_0^\infty\omega_l d\omega_l\int_0^\infty dx_1\int_0^{x_1}dx_2\int_0^{x_2}dx_3\int_0^{x_3}dx_4 i_{l_1}(\omega_k x_3)k_{l_1}(\omega_k x_1)i_{l_2}(\omega_l x_4)k_{l_2}(\omega_l x_2)$$
$$\times[R_{v\infty_1}(x_1;0,\omega_k)R_{0_1\infty_2}(x_2;\omega_k,\omega_k+\omega_l)R_{0_2\infty_3}(x_3;\omega_k+\omega_l,\omega_l)R_{0_3v}(x_4;\omega_l,0)+R_{v\infty_1}(x_1;0,\omega_k)$$
$$\times R_{0_1\infty_2}(x_2;\omega_k,\omega_k-\omega_l)R_{0_2\infty_3}(x_3;\omega_k-\omega_l,-\omega_l)R_{0_3v}(x_4;-\omega_l,0)], \tag{51}$$

where we adopt a shorthand notation $R_{ab}(x;\omega_a,\omega_b)\equiv R_{ab}(x;\epsilon_v-i\omega_a,\epsilon_v-i\omega_b)$. Removal of the constraint $\mu=\nu=0$ leads to 15 additional terms in which pairs of $R$ functions are replaced by pairs of functions denoted $P$, $Q$, and $V$, further details of which can be found in Ref. [19]. The frequency integrations were carried out using Gaussian quadrature methods. A significant complication is the fact that there is a great deal of structure in the integrand, unlike the case of the one-loop Lamb shift. In order to get adequate accuracy it was found that 28 points were needed for the $\omega_k$ integration and 23 points for the $\omega_l$ integration.

The integration of the photon frequencies still leaves five summations over angular momentum quantum numbers of the two-photon and three-electron propagators to be done. Angular momentum analysis leads to selection rules that make only two angular momentum quantum numbers independent. We choose to keep the photon angular momenta as the independent variables. Thus each overlapping diagram turns into a table of values for different values of $l_1$ and $l_2$ of the two photons.

For a given $l_1$ and $l_2$, the range of $\kappa$ values the electron propagators can take increases very rapidly, leading to a large number of channels. Table I shows the number of allowed channels for various values of $l_1$ and $l_2$ for the overlapping diagrams. Whenever possible, symmetry considerations were used to reduce the number of channels. To compute a table for $l_1=0$–5 and $l_2=0$–10, the total number of channels for a given overlapping diagram after accounting for symmetry is 3669. It is this feature of the nested and overlapping diagrams, along with the large number of points required for accurate Gaussian integration, that makes this calculation extremely computation intensive. This is in sharp contrast to the one-loop self-energy where there is one controlling $l$ and the number of channels is 2 for any given $l$.

TABLE I. Number of allowed channels for different values of $l_1$ and $l_2$ for the overlapping diagrams.

| $l_2$ | $l_1=0$ | $l_1=1$ | $l_1=2$ | $l_1=3$ | $l_1=4$ | $l_1=5$ |
|---|---|---|---|---|---|---|
| 0 | 1 | 4 | 4 | 4 | 4 | 4 |
| 1 | 4 | 36 | 36 | 40 | 40 | 40 |
| 2 | 4 | 36 | 54 | 64 | 60 | 64 |
| 3 | 4 | 40 | 64 | 100 | 96 | 104 |
| 4 | 4 | 40 | 60 | 96 | 118 | 128 |
| 5 | 4 | 40 | 64 | 104 | 128 | 164 |
| 6 | 4 | 40 | 64 | 100 | 120 | 160 |
| 7 | 4 | 40 | 64 | 104 | 128 | 168 |
| 8 | 4 | 40 | 64 | 104 | 124 | 160 |
| 9 | 4 | 40 | 64 | 104 | 128 | 168 |
| 10 | 4 | 40 | 64 | 104 | 128 | 164 |

All possible channels are computed and summed for each entry in the table. Even though we are dealing with unrenormalized diagrams that are divergent, the calculation of the individual entries in the table is well defined and finite: The divergences arise as nonconvergent $l$ sums. Specifically, at high $l_1$ or $l_2$, the entries in the table fall off as $1/l_1l_2$, so that the sum yields a $\log^2$ divergence. Such tables are constructed for the five overlapping diagrams involved in the subtraction scheme. A subtracted table is then constructed for $\Sigma_M^O$ by subtracting the individual entries in $\Sigma^{O1}$, $\Sigma^{O2}$, $\Sigma^{O3}$, $\Sigma^{O4}$, and $\Sigma^{O5}$ from $\Sigma^{4O}$.

It was found that for a given $l_1$, the $l_2$ behavior was convergent, falling off as $1/l_2^3$ for high $l_2$. Using its asymptotic behavior, the $l_2$ summation could be easily performed and it was found that at $l_1=4$ and 5, the values were falling off as $1/l_1^3$, which indicated that the final result converged. Including an estimate of the contribution of $l_1=6,\ldots,\infty$ then gives our result for the overlapping $M$ term

$$\Sigma_M^O=\begin{cases}-0.0744(1)\ \text{a.u.}, & Z=83\\ -0.0903(1)\ \text{a.u.}, & Z=92.\end{cases} \tag{52}$$

We now turn to the calculation of the nested diagram. The regulator again allows us to perform a Wick rotation without

TABLE II. Number of allowed channels for different values of $l_1$ and $l_2$ for the nested diagrams.

| $l_2$ | $l_1=0$ | $l_1=1$ | $l_1=2$ | $l_1=3$ | $l_1=4$ | $l_1=5$ | $l_1=6$ |
|---|---|---|---|---|---|---|---|
| 0 | 1 | 4 | 4 | 4 | 4 | 4 | 4 |
| 1 | 4 | 20 | 24 | 24 | 24 | 24 | 24 |
| 2 | 4 | 22 | 32 | 36 | 36 | 36 | 36 |
| 3 | 4 | 24 | 40 | 52 | 56 | 56 | 56 |
| 4 | 4 | 24 | 38 | 52 | 64 | 68 | 68 |
| 5 | 4 | 24 | 40 | 56 | 72 | 84 | 88 |
| 6 | 4 | 24 | 40 | 54 | 68 | 84 | 96 |
| 7 | 4 | 24 | 40 | 56 | 72 | 88 | 104 |
| 8 | 4 | 24 | 40 | 56 | 70 | 84 | 100 |
| 9 | 4 | 24 | 40 | 56 | 72 | 88 | 104 |
| 10 | 4 | 24 | 40 | 56 | 72 | 86 | 100 |
| 11 | 4 | 24 | 40 | 56 | 72 | 88 | 104 |
| 12 | 4 | 24 | 40 | 56 | 72 | 88 | 102 |

TABLE III. High-$l_2$ partial wave expansion when $l_1=2$ for nested diagram at $Z=92$ (in a.u.). Numbers in square brackets denote inverse multiplicative powers of 10.

| $l_2$ | $\Sigma^N$ | $\Sigma^{N1}$ | $\Sigma^{N2}$ | $\Sigma^N_M$ |
|---|---|---|---|---|
| 9 | 0.4214019003[2] | 0.4895559827[2] | −0.6844077168[3] | 0.2866892800[5] |
| 10 | 0.3850268477[2] | 0.4465280546[2] | −0.6171875836[3] | 0.2175514600[5] |
| 11 | 0.3541911225[2] | 0.4102364537[2] | −0.5621386935[3] | 0.1685381500[5] |
| 12 | 0.3277512211[2] | 0.3792394689[2] | −0.5162072232[3] | 0.1324745200[5] |
| 13 | 0.3048483893[2] | 0.3524717818[2] | −0.4772935905[3] | 0.1059665500[5] |
| 14 | 0.2848282235[2] | 0.3291313152[2] | −0.4438875358[3] | 0.8566188000[6] |
| 15 | 0.2671849497[2] | 0.3086038978[2] | −0.4148971474[3] | 0.7076664000[6] |

encountering any poles. As before, we simplify the integrand so that the photon frequencies are positive in their integration ranges. We then get for the region $x_1>x_2>x_3>x_4$ with the restriction $\mu=\nu=0$,

$$\Sigma^{4N}(I)=\frac{\alpha^2}{2\pi^2}\sum_{\kappa_{123},l_{12}}^{\kappa_3=\kappa_1}\frac{(2l_1+1)(2l_2+1)}{(2j_v+1)(2j_{\kappa_1}+1)}(-1)^{l_1+l_2+j_v+j_{\kappa_2}}C^2_{l_1}(\kappa_v\kappa_1)C^2_{l_2}(\kappa_1\kappa_2)$$
$$\times\int_0^\infty\omega_k d\omega_k\int_0^\infty\omega_l d\omega_l\int_0^\infty dx_1\int_0^{x_1}dx_2\int_0^{x_2}dx_3\int_0^{x_3}dx_4\;\; i_{l_1}(\omega_k x_4)$$
$$\times k_{l_1}(\omega_k x_1)\;\; i_{l_2}(\omega_l x_3)\;\; k_{l_2}(\omega_l x_2)\;\; [R_{v\infty_1}(x_1;0,\omega_k)R_{0_1\infty_2}(x_2;\omega_k,\omega_k+\omega_l)R_{0_2\infty_3}(x_3;\omega_k+\omega_l,\omega_k)R_{0_3v}(x_4;\omega_k,0)$$
$$+R_{v\infty_1}(x_1;0,\omega_k)R_{0_1\infty_2}(x_2;\omega_k,\omega_k-\omega_l)R_{0_2\infty_3}(x_3;\omega_k-\omega_l,\omega_k)R_{0_3v}(x_4;\omega_k,0)]. \quad (53)$$

A simplifying feature of the nested diagram is a symmetry that makes only 10 of the 24 regions of coordinate integration independent. The integration over the frequency of the inner photon was performed first, followed by the integration over the frequency of the outer photon. It was found that 30 Gaussian points were sufficient for the outer photon frequency integration and 23 for the inner photon frequency integration. As before, angular momentum analysis reduces five summations to two independent variables, which were chosen to be the photon angular momentum variables $l_1$ and $l_2$. Thus each nested diagram turns into a table of values for different values of $l_1$ and $l_2$ of the two photons.

A large number of channels are allowed for moderately high $l$. Table II shows the number of allowed channels for various values of $l_1$ and $l_2$ for the nested diagram. The nested diagram lacks the symmetry of the overlapping diagram, and it is necessary to compute the entire table instead of the upper diagonal half. To compute a table for $l_1=0$–5 and $l_2=0$–15, the total number of channels for a given diagram is 3891.

Table III shows the construction of tables for different nested diagrams at $Z=92$ for $l_1=2$. A subtracted table is then constructed for $\Sigma^N_M$ by subtracting the individual entries in $\Sigma^{N1}$ and $\Sigma^{N2}$ from $\Sigma^N$ as

$$\Sigma^N_M(l_1,l_2)=\Sigma^N(l_1,l_2)-\Sigma^{N1}(l_1,l_2)-\Sigma^{N2}(l_1,l_2). \quad (54)$$

It was found that for a given $l_1$, the $l_2$ behavior was convergent. The values at $l_2=11$ and $l_2=12$ were fitted to the polynomial $a/l_2^3+b/l_2^4$, which was then used to carry out the summation from $l_2=13$ to $\infty$. Fits using the values $l_2=13$–15 were also carried out and it was found that the extrapolation was stable to three significant digits. Having performed the $l_2$ summation, it was found that at $l_1=4$ and 5, the values were falling off as at least $1/l_1^2$, which indicated that the final result converged. Channels involving Dirac-Coulomb propagators with angular momentum $\kappa=-1$ were calculated using the $\Delta$ regulator for at least two values of $\Delta$ and fitted to the form $(\alpha/\pi)\Sigma^{(2;MP)}_{c,4}\ln\Delta+A+B\Delta$. We find

$$\Sigma^N_M=\frac{\alpha}{\pi}\Sigma^{(2;MP)}_{c,4}\;\ln\Delta+\begin{cases}0.0857(1) & \text{a.u.}, \quad Z=83\\ 0.0961(1) & \text{a.u.}, \quad Z=92.\end{cases} \quad (55)$$

At this point we discuss the amount of computation required and resources used. It took about 13 min to compute one channel of the overlapping and 12 min for the nested diagram on a single node of an IBM SP2 and a SUN UltraSPARC 1 workstation. Diagrams with a single potential interaction involve more than 24 coordinate regions and took twice the amount of computation as diagrams without any potential interaction. Thus the overlapping subtraction scheme involves the computational equivalent of six overlapping diagrams and the nested subtraction scheme involves four. Thus the total time required to perform the overlapping subtraction scheme for one value of $Z$ is (13 min per channel) × (3669 channels per overlapping diagram) × (6 overlapping diagrams) = 4770 h. The total time required for the nested subtraction scheme for one value of $Z$ is (11 min per channel) × (3891 channels per nested diagram) × (4 nested diagrams) = 2853 h. Thus the entire calculation requires 7323 h of computation for a given value of $Z$. This very large

amount of computation was performed on a Parallel Operating Environment in an IBM SP2 cluster consisting of 14 nodes and a local area multicomputer (LAM) -based parallel environment on a SUN UltraSPARC 1 cluster consisting of about 170 nodes at University of Notre Dame.

## V. SUBTRACTION TERMS

We have introduced seven subtraction terms in order to render the unrenormalized nested, overlapping, and derivative terms ultraviolet finite. The Fourier-transformed forms of the nested subtraction terms are

$$\Sigma^{N1}=-e^4\int d^3p_2d^3qd^3p_1\int\frac{d^nk}{(2\pi)^n}\frac{d^nl}{(2\pi)^n}\frac{1}{k^2+i\delta}\frac{1}{l^2+i\delta}\overline{\psi_v}(\vec{p}_2)\gamma^\mu S_F(\vec{p}_2-\vec{k},\vec{q}-\vec{k};\epsilon_v-k_0)\gamma^\nu\ \frac{1}{\not q-\not k-\not l-m}\gamma_\nu$$
$$\times S_F(\vec{q}-\vec{k},\vec{p}_1-\vec{k};\epsilon_v-k_0)\gamma_\mu\psi_v(\vec{p}_1) \tag{56}$$

and

$$\Sigma^{N2}=e^4\frac{Z\alpha}{2\pi^2}\int\frac{d^3p_2d^3q_2d^3q_1d^3p_1}{|\vec{q}_2-\vec{q}_1|^2}\int\frac{d^nk}{(2\pi)^n}\frac{d^nl}{(2\pi)^n}\frac{1}{k^2+i\delta}\frac{1}{l^2+i\delta}\overline{\psi_v}(\vec{p}_2)\gamma^\mu S_F(\vec{p}_2-\vec{k},\vec{q}_2-\vec{k};\epsilon_v$$
$$-k_0)\gamma^\nu\ \frac{1}{\not q_2-\not k-\not l-m}\gamma_0\frac{1}{\not q_1-\not k-\not l-m}\gamma_\nu S_F(\vec{q}_1-\vec{k},\vec{p}_1-\vec{k};\epsilon_v-k_0)\gamma_\mu\psi_v(\vec{p}_1). \tag{57}$$

Similarly, the overlapping subtraction terms are

$$\Sigma^{O1}=-e^4\int d^3p_2d^3p_1\int\frac{d^nk}{(2\pi)^n}\frac{d^nl}{(2\pi)^n}\frac{1}{k^2+i\delta}\frac{1}{l^2+i\delta}\overline{\psi_v}(\vec{p}_2)\gamma^\mu S_F(\vec{p}_2-\vec{k},\vec{p}_1-\vec{k};\epsilon_v-k_0)$$
$$\times\gamma^\nu\frac{1}{\not p_1-\not k-\not l-m}\gamma_\mu\frac{1}{\not p_1-\not l-m}\gamma_\nu\psi_v(\vec{p}_1), \tag{58}$$

$$\Sigma^{O2}=-e^4\int d^3p_2d^3p_1\int\frac{d^nk}{(2\pi)^n}\frac{d^nl}{(2\pi)^n}\frac{1}{k^2+i\delta}\frac{1}{l^2+i\delta}\overline{\psi_v}(\vec{p}_2)\gamma^\mu\frac{1}{\not p_2-\not k-m}\gamma^\nu\frac{1}{\not p_2-\not k-\not l-m}\gamma_\mu S_F(\vec{p}_2-\vec{k},\vec{p}_1-\vec{k};\epsilon_v-k_0)$$
$$\times\gamma_\nu\psi_v(\vec{p}_1), \tag{59}$$

$$\Sigma^{O3}=-e^4\int d^3p\int\frac{d^nk}{(2\pi)^n}\frac{d^nl}{(2\pi)^n}\frac{1}{k^2+i\delta}\frac{1}{l^2+i\delta}\overline{\psi_v}(\vec{p})\gamma^\mu\frac{1}{\not p-\not k-m}\gamma^\nu\frac{1}{\not p-\not k-\not l-m}\gamma_\mu\frac{1}{\not p-\not l-m}\gamma_\nu\psi_v(\vec{p}), \tag{60}$$

and

$$\Sigma^{O4}=8\alpha^2(Z\alpha)\int\frac{d^3p_2d^3p_1}{|\vec{p}_2-\vec{p}_1|^2}\int\frac{d^nk}{(2\pi)^n}\int\frac{d^nl}{(2\pi)^n}\frac{1}{k^2+i\delta}\frac{1}{l^2+i\delta}\overline{\psi_v}(\vec{p}_2)\gamma_\mu\frac{1}{\not p_2-\not k-m}\gamma_\nu\frac{1}{\not p_2-\not k-\not l-m}$$
$$\times\gamma_0\frac{1}{\not p_1-\not k-\not l-m}\gamma^\mu\frac{1}{\not p_1-\not l-m}\gamma^\nu\psi_v(\vec{p}_1). \tag{61}$$

Finally, the derivative subtraction term is

$$\Sigma^{D1}=ie^2\Sigma_c^{(2)}\int d^3p\ \int\frac{d^nl}{(2\pi)^n}\frac{1}{l^2+i\delta}\overline{\psi_v}(\vec{p})\gamma_\mu\frac{1}{\not p-\not l-m}\gamma_0\frac{1}{\not p-\not l-m}\gamma^\mu\psi_v(\vec{p}). \tag{62}$$

Because $\Sigma^{O1}$ is equal to $\Sigma^{O2}$, we will account for the latter term by doubling the former in the following. We note that in all of the subtraction terms the $d^nl$ integration can be carried out with Feynman parameter techniques, leading to the functions defined in Sec. I A. Thus these diagrams can be thought of as generalizations of the one-loop Lamb shift. We first consider the subtraction terms that contain Dirac-Coulomb propagators, $\Sigma^{N1}$, $\Sigma^{N2}$, and $2\Sigma^{O1}$. After carrying out the $d^nl$ integration, they can be split into two parts, one of which involves the constants $\widetilde{B}^{(2)}$ and $\widetilde{L}^{(2)}$ and the other the functions $\Sigma_c^{2:0P}(q-k)$ and $\Lambda_{c\rho}^{(2)}(p_2-k,p_1-k)$. The former parts can be grouped together into a single term and we can write

$$\Sigma^{N1}+\Sigma^{N2}+\Sigma^{O1}+\Sigma^{O2}=\widetilde{L}^{(2)}[\,\delta m^{(2)}+\Sigma_c^{(2)}]-ie^2\int d^3p_2d^3qd^3p_1\int\frac{d^nk}{(2\pi)^n}\frac{1}{k^2+i\delta}\overline{\psi_v}(\vec{p}_2)\,\gamma^\mu S_F(\vec{p}_2-\vec{k},\vec{q}-\vec{k};\epsilon_v-k_0)$$
$$\times\Sigma_c^{2:0P}(q-k)S_F(\vec{q}-\vec{k},\vec{p}_1-\vec{k};\epsilon_v-k_0)\,\gamma_\mu\psi_v(\vec{p}_1)$$
$$+ie^2\frac{Z\alpha}{2\pi^2}\int\frac{d^3p_2d^3q_2d^3q_1d^3p_1}{|\vec{q}_2-\vec{q}_1|^2}\int\frac{d^nk}{(2\pi)^n}\frac{1}{k^2+i\delta}\overline{\psi_v}(\vec{p}_2)\,\gamma^\mu S_F(\vec{p}_2-\vec{k},\vec{q}_2-\vec{k};\epsilon_v-k_0)$$
$$\times\Lambda_{c0}^{(2)}(q_2-k,q_1-k)S_F(\vec{q}_1-\vec{k},\vec{p}_1-\vec{k};\epsilon_v-k_0)\,\gamma_\mu\psi_v(\vec{p}_1)$$
$$-2ie^2\int d^3p_2d^3p_1\int\frac{d^nk}{(2\pi)^n}\frac{1}{k^2+i\delta}\overline{\psi_v}(\vec{p}_2)$$
$$\times\gamma^\mu S_F(\vec{p}_2-\vec{k},\vec{p}_1-\vec{k};\epsilon_v-k_0)\Lambda_{c\mu}^{(2)}(p_1-k,p_1)\psi_v(\vec{p}_1). \tag{63}$$

The first term was obtained by using the equation for the Dirac-Coulomb propagator together with the Ward identity $\widetilde{B}^{(2)}=-\widetilde{L}^{(2)}$. Note that $\widetilde{L}^{(2)}$ multiplies the unrenormalized one-loop Lamb shift: The $\delta m^{(2)}$ part of this forms part of the two-loop mass renormalization counterterm $\delta m^{(4)}$.

While $\Sigma_c^{2:0P}(q-k)$ and $\Lambda_{c\rho}^{(2)}(p_2-k,p_1-k)$ are finite quantities, they lead to $1/\epsilon^2$ and $1/\epsilon$ divergences when the $d^nk$ integration is carried out. However, these divergences are associated with the 0P and 1P parts of the Dirac-Coulomb propagators. Thus we can define an ultraviolet finite expression, the $P$ term, as $\Sigma_P=\Sigma_P^{N1}+\Sigma_P^{N2}+2\Sigma_P^{O1}$, with

$$\Sigma_P^{N1}\equiv-ie^2\int d^3p_2d^3qd^3p_1\int\frac{d^nk}{(2\pi)^n}\frac{1}{k^2+i\delta}\overline{\psi_v}(\vec{p}_2)\,\gamma^\mu[S_F(\vec{p}_2-\vec{k},\vec{q}-\vec{k};\epsilon_v-k_0)\Sigma_{c,4}^{2:0P}(q-k)S_F(\vec{q}-\vec{k},\vec{p}_1-\vec{k};\epsilon_v-k_0)$$
$$-S_0(\vec{p}_2-\vec{k},\vec{q}-\vec{k};\epsilon_v-k_0)\Sigma_{c,4}^{2:0P}(q-k)S_0(\vec{q}-\vec{k},\vec{p}_1-\vec{k};\epsilon_v-k_0)-S_0(\vec{p}_2-\vec{k},\vec{q}-\vec{k};\epsilon_v-k_0)\Sigma_{c,4}^{2:0P}(q-k)$$
$$\times S_1(\vec{q}-\vec{k},\vec{p}_1-\vec{k};\epsilon_v-k_0)-S_1(\vec{p}_2-\vec{k},\vec{q}-\vec{k};\epsilon_v-k_0)\Sigma_{c,4}^{2:0P}(q-k)S_0(\vec{q}-\vec{k},\vec{p}_1-\vec{k};\epsilon_v-k_0)]\,\gamma_\mu\psi_v(\vec{p}_1), \tag{64}$$

$$\Sigma_P^{N2}\equiv ie^2\frac{Z\alpha}{2\pi^2}\int\frac{d^3p_2d^3q_2d^3q_1d^3p_1}{|\vec{q}_2-\vec{q}_1|^2}\int\frac{d^nk}{(2\pi)^n}\frac{1}{k^2+i\delta}\overline{\psi_v}(\vec{p}_2)\,\gamma^\mu[S_F(\vec{p}_2-\vec{k},\vec{q}_2-\vec{k};\epsilon_v-k_0)\Lambda_{c40}^{(2)}(q_2-k,q_1-k)$$
$$\times S_F(\vec{q}_1-\vec{k},\vec{p}_1-\vec{k};\epsilon_v-k_0)-S_0(\vec{p}_2-\vec{k},\vec{q}_2-\vec{k};\epsilon_v-k_0)\Lambda_{c40}^{(2)}(q_2-k,q_1-k)S_0(\vec{q}_1-\vec{k},\vec{p}_1-\vec{k};\epsilon_v-k_0)]\,\gamma_\mu\psi_v(\vec{p}_1), \tag{65}$$

and

$$2\Sigma_P^{O1}\equiv-2ie^2\int d^3p_2d^3p_1\int\frac{d^nk}{(2\pi)^n}\frac{1}{k^2+i\delta}\overline{\psi_v}(\vec{p}_2)\,\gamma^\mu[S_F(\vec{p}_2-\vec{k},\vec{p}_1-\vec{k};\epsilon_v-k_0)-S_0(\vec{p}_2-\vec{k},\vec{p}_1-\vec{k};\epsilon_v-k_0)$$
$$-S_1(\vec{p}_2-\vec{k},\vec{p}_1-\vec{k};\epsilon_v-k_0)]\Lambda_{c4\mu}^{(2)}(p_1-k,p_1)\psi_v(\vec{p}_1). \tag{66}$$

The diagrammatic version of these equations is given in Fig. 4. The subtractions we have introduced force there to be at least two interactions with the external potential present, which makes the above terms ultraviolet finite. While finite, they involve the Dirac-Coulomb propagator in momentum space. We will discuss an approach to the calculation of the $P$ terms in the conclusion, but do not analyze them further here.

At this point we can define the third part of the calculation, $\Sigma_F$, defined through $\Sigma^{4SE}=\Sigma_M+\Sigma_P+\Sigma_F$. Putting together Eqs. (29), (39), (41)–(43), and (63)–(66), we have

$$\Sigma_F=\widetilde{L}^{(2)}C\Sigma_c^{(2:MP)}+\Sigma^{O3}+\Sigma^{O4}+\Sigma^{D1}+\Sigma^{N:0P}+2\Sigma^{N:\mathrm{side}}+\Sigma^{N:\mathrm{ladder}}+2\Sigma^{O:\mathrm{corner}}. \tag{67}$$

We have introduced here four new terms $\Sigma^{N:0P}$,$\Sigma^{N:\mathrm{side}}$,$\Sigma^{N:\mathrm{ladder}}$, and $\Sigma^{O:\mathrm{corner}}$, which are represented in Figs. 5(a)–5(d), respectively. The names ''side,'' ''ladder,'' and ''corner'' are chosen to follow the notation of Ref. [5]. We note that in the first two diagrams the self-mass counterterm is understood to be included. Along with $\Sigma^{O3}$ and $\Sigma^{O4}$, which are given in Figs. 5(e) and 5(f), they represent all bare nested and overlapping Feynman diagrams with zero or one external interaction. These diagrams are related to the subtractions that define the $P$ term by replacing either $\Sigma_c^{(2)}(p)$ by $\Sigma^{(2)}(p)-\widetilde{B}^{(2)}(\not{p}-m)$ or $\Lambda_{c\rho}^{(2)}(p_1,p_2)$ by $\Lambda_\rho(p_1,p_2)-\widetilde{L}^{(2)}\gamma_\rho$. The expressions for these last terms are

$$\Sigma^{4N:0P}=-16\pi^2\alpha^2\int d^3p\int\frac{d^nk}{(2\pi)^n}\int\frac{d^nl}{(2\pi)^n}\overline{\psi_v}(\vec{p})\,\gamma_\mu\frac{1}{\not{p}-\not{k}-m}\gamma_\nu\frac{1}{\not{p}-\not{k}-\not{l}-m}\gamma^\nu\frac{1}{\not{p}-\not{k}-m}\,\gamma^\mu\psi_v(\vec{p}), \tag{68}$$

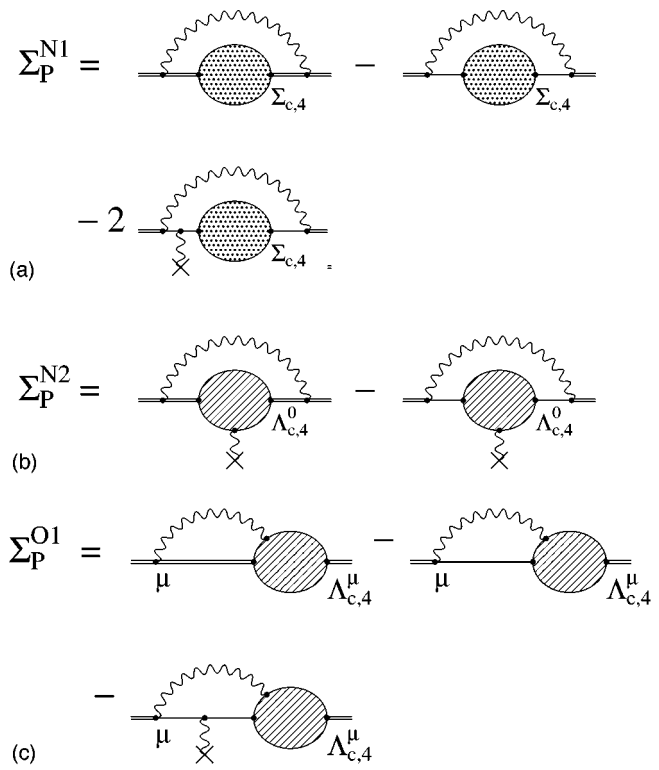


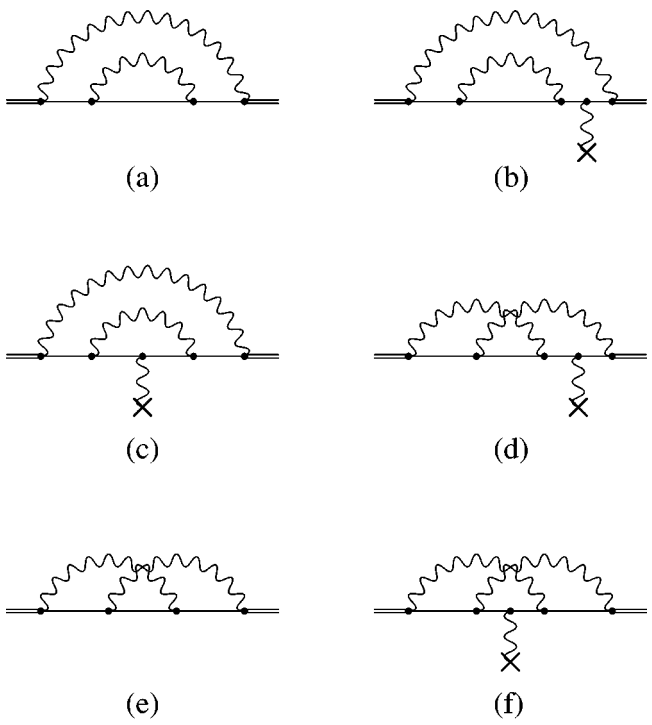


FIG. 5. Diagrams contributing to the $F$ term.

FIG. 4. Diagrammatic representation of the subtraction scheme that defines the $P$ term.

$$\Sigma^{\text{side}} = 8\alpha^2(Z\alpha)\int \frac{d^3p_2 d^3p_1}{|\vec{p}_2-\vec{p}_1|^2}\int \frac{d^nk}{(2\pi)^n}\int \frac{d^nl}{(2\pi)^n}\,\frac{1}{k^2}\,\frac{1}{l^2}\,\overline{\psi_v}(\vec{p}_2)\,\gamma_\mu \frac{1}{\not p_2-\not k-m}\gamma_\nu \frac{1}{\not p_2-\not k-\not l-m}\,\gamma^\nu \frac{1}{\not p_2-\not k-m}$$
$$\times \gamma_0 \frac{1}{\not p_1-\not k-m}\,\gamma^\mu \psi_v(\vec{p}_1), \tag{69}$$

$$\Sigma^{\text{ladder}} = 8\alpha^2(Z\alpha)\int \frac{d^3p_2 d^3p_1}{|\vec{p}_2-\vec{p}_1|^2}\int \frac{d^nk}{(2\pi)^n}\int \frac{d^nl}{(2\pi)^n}\,\frac{1}{k^2}\,\frac{1}{l^2}\,\overline{\psi_v}(\vec{p}_2)\,\gamma_\mu \frac{1}{\not p_2-\not k-m}\gamma_\nu \frac{1}{\not p_2-\not k-\not l-m}\,\gamma_0 \frac{1}{\not p_1-\not k-\not l-m}$$
$$\times \gamma^\nu \frac{1}{\not p_1-\not k-m}\,\gamma^\mu \psi_v(\vec{p}_1), \tag{70}$$

and

$$\Sigma^{\text{corner}} = 8\alpha^2(Z\alpha)\int \frac{d^3p_2 d^3p_1}{|\vec{p}_2-\vec{p}_1|^2}\int \frac{d^nk}{(2\pi)^n}\int \frac{d^nl}{(2\pi)^n}\,\frac{1}{k^2}\,\frac{1}{l^2}\,\overline{\psi_v}(\vec{p}_2)\,\gamma_\mu \frac{1}{\not p_2-\not k-m}\gamma_\nu \frac{1}{\not p_2-\not k-\not l-m}$$
$$\times \gamma^\mu \frac{1}{\not p_2-\not l-m}\gamma_0 \frac{1}{\not p_1-\not l-m}\,\gamma^\nu \psi_v(\vec{p}_1). \tag{71}$$

We will now show that $\Sigma_F$ contains a self-mass term, but that the other divergences cancel, as was the case for the one-loop self-energy.

## VI. EVALUATION OF $F$ TERMS

The evaluation of the $F$ terms can be carried out using standard Feynman parameter techniques coupled with the numerical integration program VEGAS [21]. Our strategy is to first isolate the fourth-order self-mass term by setting $\not p = m, p^2 = m^2$. We will show that this term is in agreement with a Yennie gauge calculation by Adkins and Zhang [22]. After this term is removed by the fourth-order self-energy counterterm, divergences of order $1/\epsilon^2$ and $1/\epsilon$ remain in individual diagrams. Some of these divergences are proportional to $\not p - m$, but others multiply nontrivial functions of $p$. These can be identified with the 0P and

TABLE IV. Finite parts of $F$ terms (in a.u.).

| Z | $\Sigma_{c,4}^{4N:0P}$ | $\Sigma_{c,4}^{O3}$ | $\Sigma_{c,4}^{D}$ | $\Sigma_{c,4}^{O4}$ | $\Sigma_{c,4}^{\text{corner}}$ | $\Sigma_{c,4}^{\text{ladder}}$ | $\Sigma_{c,4}^{\text{side}}$ | Total |
|---|---|---|---|---|---|---|---|---|
| 10 | −0.00346 | 0.00520 | 0.00152 | −0.00121 | −0.00169 | 0.00051 | 0.00193 | 0.00280 |
| 25 | −0.00836 | 0.01279 | 0.00643 | −0.00367 | −0.00160 | 0.00111 | 0.00162 | 0.00832 |
| 50 | −0.00897 | 0.02055 | 0.01692 | −0.00866 | −0.00002 | 0.00219 | −0.00402 | 0.01799 |
| 75 | −0.00125 | 0.02695 | 0.02781 | −0.01917 | −0.00358 | 0.00115 | −0.00669 | 0.02522 |
| 83 | 0.00215 | 0.03016 | 0.03154 | −0.02545 | −0.00787 | −0.00007 | −0.00405 | 0.02641 |
| 92 | 0.00565 | 0.03611 | 0.03641 | −0.03594 | −0.01727 | −0.00273 | 0.00400 | 0.02623 |
| 100 | 0.00715 | 0.04604 | 0.04215 | −0.05027 | −0.03360 | −0.00762 | 0.01984 | 0.02369 |

1P parts of the one-loop Lamb shift and will combine with the first term of Eq. (67). After this combination, an ultraviolet finite expression for the $F$ term results.

### A. All-free diagrams

An analysis of the nested all-free diagram gives

$$\Sigma^{4N:0P}=\delta m^{(4N)}\int d^3p\ \overline{\psi_v}(\vec{p})\psi_v(\vec{p})+\widetilde{B}^{4N}\int d^3p\ \overline{\psi_v}(\vec{p})(\not{p}-m)\psi_v(\vec{p})-\frac{\alpha D}{2\pi\epsilon}\Sigma_{c,4}^{(2:0P)}+\Sigma_{c,4}^{4N:0P}, \tag{72}$$

where

$$\delta m^{(4N)}=-\frac{m\alpha^2}{\pi^2}\left[\frac{15D}{8\epsilon^2}+\frac{55D}{32\epsilon}-\frac{27}{32}\zeta(2)+\frac{197}{128}\right], \tag{73}$$

$$\widetilde{B}^{4N}=\frac{\alpha^2}{\pi^2}\left[\frac{D}{8\epsilon^2}+\frac{D}{32\epsilon}\right], \tag{74}$$

and

$$D=(4\pi)^{\epsilon}\Gamma(1+\epsilon). \tag{75}$$

$\Sigma_{c,4}^{4N:0P}$ is tabulated in the second column of Table IV.

The overlapping all-free diagram is given by

$$\Sigma^{O3}=\delta m^{(4O)}\int d^3p\ \overline{\psi_v}(\vec{p})\psi_v(\vec{p})+\widetilde{B}^{(4O)}\int d^3p\ \overline{\psi_v}(\vec{p})(\not{p}-m)\psi_v(\vec{p})+\frac{\alpha D}{\pi\epsilon}\Sigma_{c,4}^{(2:0P)}+\Sigma_{c,4}^{O3}, \tag{76}$$

where

$$\delta m^{(4O)}=\frac{m\alpha^2}{\pi^2}\left[\frac{3D}{4\epsilon^2}+\frac{5D}{16\epsilon}-0.375\,635(9)\right] \tag{77}$$

and

$$\widetilde{B}^{(4O)}=-\frac{\alpha^2}{\pi^2}\left[\frac{D}{4\epsilon^2}-\frac{D}{16\epsilon}\right]. \tag{78}$$

$\Sigma_{c,4}^{O3}$ is tabulated in the third column of Table IV. Putting together the fourth-order self-mass from the nested and overlapping diagrams gives

$$\delta m^{(4)}=\frac{m\alpha^2}{\pi^2}\left[-\frac{9D}{8\epsilon^2}-\frac{45D}{32\epsilon}-0.526\,78(1)\right]. \tag{79}$$

The constant has been evaluated by Adkins and Zhang [22] to be $3/4\zeta(3)-3\zeta(2)\ln 2+69/32\zeta(2)-199/128$, consistent with our numerical determination. We note that although the analytic calculation was carried out in Yennie gauge, the agreement follows from the gauge invariance of the self-mass. However, the constants $\widetilde{B}^{(4N)}$ and $\widetilde{B}^{(4O)}$ are gauge variant, and differ from the Yennie gauge calculation. The self-mass term is removed by the fourth-order mass renormalization counterterm.

### B. Derivative term

The derivative term is related to the one-loop vertex function introduced in Sec. I A through

$$\Sigma^{D1} = -\Sigma_c^{(2)} \int d^3p \ \overline{\psi_v}(\vec{p}) \Lambda_0^{(2)}(p,p) \psi_v(\vec{p}). \tag{80}$$

Using Eq. (9) then leads to

$$\Sigma^{D1} = -\widetilde{L}^{(2)} \Sigma_c^{(2)} + \Sigma_{c,4}^{D1}, \tag{81}$$

with

$$\Sigma_{c,4}^{D1} = \frac{\alpha}{2\pi} \Sigma_{c,4}^{(2)} + \frac{\alpha}{2\pi} \Sigma_{c,4}^{(2)} \int d^3p \ \overline{\psi_v}(\vec{p}) \gamma^0 \psi_v(\vec{p}) \int_0^1 \rho \ d\rho \ln[\rho - \rho(1-\rho)p^2/m^2]$$
$$+ \frac{\alpha}{4\pi} \Sigma_{c,4}^{(2)} \int d^3p \int_0^1 \rho \ d\rho \frac{\overline{\psi_v}(\vec{p}) \gamma^\mu [(1-\rho)\not{p} + m] \gamma^0 [(1-\rho)\not{p} + m] \gamma_\mu \psi_v(\vec{p})}{m^2\rho - \rho(1-\rho)p^2}. \tag{82}$$

Inserting Eq. (20) into the first term in Eq. (81) gives

$$-\widetilde{L}^{(2)} \Sigma_c^{(2)} = -\frac{\alpha C^2}{2\pi\epsilon} (\Sigma_{c,4}^{(2:0P)} + \Sigma_{c,4}^{(2:1P)} + \Sigma_c^{(2:MP)} + \epsilon \Sigma_{c,\epsilon}^{(2:0P)}$$
$$+ \epsilon \Sigma_{c,\epsilon}^{(2:1P)}) = -\frac{\alpha D}{2\pi\epsilon} (\Sigma_{c,4}^{(2:0P)} + \Sigma_{c,4}^{(2:1P)}$$
$$+ \Sigma_c^{(2:MP)}) - \frac{\alpha}{2\pi} (\Sigma_{c,\epsilon}^{(2:0P)} + \Sigma_{c,\epsilon}^{(2:1P)}). \tag{83}$$

Note that both $\widetilde{L}^{(2)}$ and $\Sigma_c^{(2)}$ involve a factor of $C$. Since to order $\epsilon$, $C^2 = D$, the above expression involves $D$ where we have specified that $\Sigma_{c,\epsilon}^{2:0P}$ and $\Sigma_{c,\epsilon}^{2:1P}$ do not involve Taylor expanding the constant $C$. We hold the first bracket for later combination with other terms and the finite remainder is added to $\Sigma_{c,4}^{D1}$ and tabulated in the fourth column of Table IV.

### C. One-potential diagrams

We begin with the least divergent one-potential diagram $\Sigma^{O4}$. We define the finite residue through

$$\Sigma^{O4} = \widetilde{L}^{O4} \int d^3p \ \overline{\psi_v}(\vec{p}) (\not{p} - m) \psi_v(\vec{p}) + \Sigma_{c,4}^{O4}, \tag{84}$$

where

$$\widetilde{L}^{O4} = -\frac{\alpha^2 D}{4\pi^2 \epsilon}. \tag{85}$$

The finite term is tabulated in the fifth column of Table IV.

Turning to the corner diagram, we define its finite residue through

$$2\Sigma^{\text{corner}} = \widetilde{L}^{\text{corner}} \int d^3p \ \overline{\psi_v}(\vec{p}) (\not{p} - m) \psi_v(\vec{p})$$
$$+ \frac{\alpha D}{\pi\epsilon} \Sigma_{c,4}^{(2:1P)} + \Sigma_{c,4}^{\text{corner}}, \tag{86}$$

where

$$\widetilde{L}^{\text{corner}} = \frac{\alpha^2 D}{\pi^2} \left( \frac{1}{4\epsilon^2} + \frac{3}{16\epsilon} \right). \tag{87}$$

$\Sigma_{c,4}^{\text{corner}}$ is tabulated in the sixth column of Table IV.

The ladder diagram is

$$\Sigma^{\text{ladder}} = \widetilde{L}^{\text{ladder}} \int d^3p \ \overline{\psi_v}(\vec{p}) (\not{p} - m) \psi_v(\vec{p})$$
$$+ \frac{\alpha D}{2\pi\epsilon} \Sigma_{c,4}^{(2:1P)} + \Sigma_{c,4}^{\text{ladder}}, \tag{88}$$

where

$$\widetilde{L}^{\text{ladder}} = \frac{\alpha^2 D}{\pi^2} \left( \frac{1}{8\epsilon^2} + \frac{5}{32\epsilon} \right). \tag{89}$$

$\Sigma_{c,4}^{\text{ladder}}$ is tabulated in the seventh column of Table I.

Finally, the expression for the side diagram is

$$2\Sigma^{\text{side}} = \widetilde{L}^{\text{side}} \int d^3p \ \overline{\psi_v}(\vec{p}) (\not{p} - m) \psi_v(\vec{p})$$
$$- \frac{\alpha D}{\pi\epsilon} \Sigma_{c,4}^{2:1P} + \Sigma_{c,4}^{\text{side}}, \tag{90}$$

where

$$\widetilde{L}^{\text{side}} = \frac{\alpha^2 D}{\pi^2} \left( -\frac{1}{4\epsilon^2} - \frac{3}{16\epsilon} \right). \tag{91}$$

The finite term is tabulated in the eighth column of Table IV.

We can now group together all the terms contributing to the $F$ term. The finite terms are summed in the last column of Table IV. The derivative term plays a central role in canceling the remaining divergences. Specifically, we have the divergent part of the derivative term from Eq. (83) as

$$\Sigma_{\text{divergent}}^{D1} = -\frac{\alpha D}{2\pi\epsilon} [\Sigma_{c,4}^{(2:0P)} + \Sigma_{c,4}^{(2:1P)} + \Sigma_c^{(2:MP)}]. \tag{92}$$

The first term can be seen to exactly cancel similar divergences in Eqs. (72) and (76) and the second the divergences from Eqs. (84), (86), (88), and (90). The many-potential term then cancels with the first term in the definition of $\Sigma_F$ given in Eq. (67). We also note that the Ward identities for the nested and overlap diagrams are satisfied through

$$\widetilde{B}^{4N} = -[\widetilde{L}^{\text{ladder}} + \widetilde{L}^{\text{side}}], \tag{93}$$

$$\widetilde{B}^{4O} = -[\widetilde{L}^{O4} + \widetilde{L}^{\text{corner}}]. \tag{94}$$

At this point all ultraviolet divergences have been removed, either by cancellation between various terms or through mass renormalization. We note that we have dealt only with unrenormalized graphs in this treatment. It is also possible to work with renormalized graphs throughout; however, it is simple to show that the wave-function renormalization and vertex renormalization counterterm graphs cancel separately, so the end result would remain unchanged.

The $F$ term does not demonstrate a $Z^4$ scaling at high $Z$ and is in fact relatively constant between 50 and 100. However, such scaling is not to be expected, given the behavior of Eq. (2), except at very low $Z$. As alluded to in the Introduction, the value of the $F$ term at $Z=92$ is about 1 eV, specifically 0.714 eV. However, because we have not evaluated the $P$ term, the calculation is incomplete and we cannot make predictions for experiment. However, the finite parts of the $M$ term (the reference-state singularity will cancel with the $P$ term) sum to $-1.039$ eV at $Z=92$, so if the finite part of the $P$ term happens to be small, after adding the $-0.971$ eV PO contribution [4], the fourth-order self-energy shift would be $-1.296$ eV. While a shift of this size would be difficult to detect in hydrogenlike uranium, it may be measurable in the spectra of many-electron ions, though, as discussed in the Introduction, additional QED diagrams will have to be calculated.

## VII. DISCUSSION

A major feature of exact calculations of the Lamb shift is the differing roles of coordinate space and momentum space. If the calculation were ultraviolet finite, coordinate space would be favored, as the behavior of the Dirac-Coulomb Green's function is well known both analytically and numerically in coordinate space. However, divergences are most easily treated with covariant methods in momentum space. In the case of the one-loop self-energy, this is illustrated by the fact that subtractions involving free-electron propagators are made in coordinate space, leading to a convergent term represented by a partial wave expansion, while the subtractions themselves are analyzed by Fourier transforming to momentum space, where the self-mass infinity is easily removed and divergences related to wave function and vertex renormalization shown to cancel.

The situation is somewhat more complex in the two-loop case. One of our principal results is that subtractions can be devised in coordinate space that lead to the same kind of convergent partial wave expansions as in the one-loop case, although the amount of computer time required for an accurate evaluation is much greater. However, the subtraction terms, when Fourier transformed to momentum space, of necessity involve not only free propagators, but also Dirac-Coulomb propagators. While we have been able to introduce additional subtractions that make the expressions involving these propagators ultraviolet finite, the numerical analysis of the resulting $P$ terms has not been carried out. The reason for this is the fact that the Dirac-Coulomb propagator is generally treated in coordinate space and less is known about it in momentum space. This is in contrast to the situation with the nonrelativistic propagator, which is known in both coordinate and momentum space [23]. One possible approach is to Fourier transform the $P$ term back into coordinate space. However, we are presently exploring another approach using the spectral decomposition of the electron propagator. While Green's-functions techniques have a number of advantages, we note that the work of Blundell and Snyderman [14] involved the isolation of the many-potential term, which was then evaluated using basis sets based on $B$ splines. We are presently developing a relativistic basis set, again based on $B$ splines, but in this case in momentum space. With such a basis set, the integrals involved in the $P$ terms could be treated entirely in momentum space.

Once the $P$ terms are evaluated it will be possible to systematically study the $Z$ dependence of the two-loop self-energy. While we have discussed in the Introduction the importance of such a study for highly charged ions such as lithiumlike bismuth, there is another important application at low $Z$. That is the determination through fitting procedures of the higher-order terms in Eq. (2). In a recent calculation of one-loop radiative corrections to hyperfine splitting [24], it was shown that by calculating radiative corrections to all orders in $Z\alpha$ for a range of $Z$ the first coefficients of the series expansion could be verified and at the same time all higher-order terms in the series obtained. An important goal of the present calculation is the extension to lower values of $Z$. Given the large coefficient of the order $Z\alpha$ term in Eq. (2), it is quite possible that the next term, and conceivably even higher-order terms, could enter at the level of experimental interest even at $Z=1$ or $Z=2$. By carrying out calculations such as that described in this paper that are valid to all orders in $Z\alpha$, the questions of how important these higher-order terms are and what their implications are for QED tests at low $Z$ can be answered.

## ACKNOWLEDGMENTS

This work was supported in part by NSF Grant No. PHY-95-13179. Particular thanks are due to S. A. Blundell for the introduction of the method of regulating reference state singularities, K. T. Cheng, who played a principal role in developing a great deal of the numerical techniques used in the calculation, and P. Beiersdorfer and A. E. Livingston for conversations about the experimental situation. In addition, we gratefully acknowledge the computational resources provided by the Office of Information Technologies at Notre Dame, made available by a grant from IBM.

[1] S. Mallampalli and J. Sapirstein, Phys. Rev. A **54**, 2714 (1996): a similar calculation is given by H. Persson *et al.*, *ibid.* **54**, 2805 (1996).
[2] K. Pachucki, Phys. Rev. A **48**, 2609 (1993); M. I. Eides and H. Grotch, Phys. Lett. B **308**, 389 (1993).
[3] J. A. Fox and D. R. Yennie, Ann. Phys. (N.Y.) **81**, 438 (1973).
[4] A. Mitrushenkov, L. N. Labzowsky, I. Lindgren, H. Persson, and S. Salomonson, Phys. Lett. A **200**, 51 (1995).
[5] T. Appelquist and S. J. Brodsky, Phys. Rev. A **2**, 2293 (1970).
[6] K. Pachucki, Phys. Rev. Lett. **72**, 3154 (1994); M. I. Eides and V. Shelyuto, Phys. Rev. A **52**, 954 (1995).
[7] H. F. Beyer *et al.*, Z. Phys. D **35**, 169 (1995).
[8] S. A. Blundell, Phys. Rev. A **47**, 1790 (1993).
[9] J. Schweppe *et al.*, Phys. Rev. Lett. **66**, 1434 (1991).
[10] P. Beiersdorfer *et al.*, Phys. Rev. Lett. (to be published).
[11] G. E. Brown, J. S. Langer, and G. W. Schaefer, Proc. R. Soc. London, Ser. A **251**, 92 (1959).
[12] A. Desiderio and W. R. Johnson, Phys. Rev. **3**, 1267 (1971).
[13] P. J. Mohr, Ann. Phys. (N.Y.) **88**, 26 (1974).
[14] S. A. Blundell and N. Snyderman, Phys. Rev. A **44**, R1427 (1991).
[15] K. T. Cheng, W. R. Johnson, and J. Sapirstein, Phys. Rev. A **47**, 1817 (1993).
[16] I. Lindgren, H. Persson, S. Salomonson, and A. Ynnerman, Phys. Rev. A **47**, R4555 (1993).
[17] L. N. Labzowsky and A. O. Mitrushenkov, Phys. Rev. A **53**, 3029 (1996); L. N. Labzowsky and A. O. Mitrushenkov, Phys. Lett. A **198**, 333 (1995).
[18] R. Mills and N. Kroll, Phys. Rev. **98**, 1489 (1955).
[19] S. A. Blundell, K. T. Cheng, and J. Sapirstein, Phys. Rev. A **2**, 2293 (1997).
[20] S. A. Blundell, W. R. Johnson, P. J. Mohr, and J. Sapirstein, Phys. Rev. A **48**, 2615 (1993).
[21] G. P. Lepage, J. Comput. Phys. **27**, 192 (1978).
[22] G. S. Adkins and Y. Zhang (unpublished).
[23] J. Schwinger, J. Math. Phys. **5**, 1606 (1964); L. Hostler, *ibid.* **5**, 1235 (1964).
[24] S. A. Blundell, K. T. Cheng, and J. Sapirstein, Phys. Rev. Lett. **78**, 4914 (1997).